Calvo-Rivera, A., Huete, C. & Velikovich, A. L. (2022, abril). The stability of expanding reactive shocks in a van der Waals fluid. Physics of Fluids, 34(4), 046106.

DOI: 10.1063/5.0087073

The stability of expanding reactive shocks in a van der Waals fluid

A. Calvo-Rivera,[1] C. Huete,[1] and A.L. Velikovich[2]
[1)] *Grupo de Mecánica de Fluidos, Universidad Carlos III, 28911, Leganés, Spain*[a)]
[2)] *Plasma Physics Division, Naval Research Laboratory, Washington, DC 20375, USA*

(Dated: 8 March 2022)

Despite the extensive literature accumulated since the pioneering works of D'yakov and Kontorovich in the 1950s, the stability of steady shocks is still an open question when realistic boundary conditions are accounted. The consideration of a supporting mechanism, which is indeed a necessary condition for shock steadiness, modifies the perturbation shock dynamics in the unstable range. The Noh problem is a suitable example to form steady expanding shocks. This configuration is of great interest to the high-energy-density-physics community because of its direct application to inertial confinement fusion and astrophysics, for which the stagnation of a supersonically converging material via an accretion shock front is ubiquitous. In this work, we extend the generalized Noh problem, both base-flow solution and linear stability analysis, to conditions where endothermic or exothermic transformations undergo across the shock. Within the spontaneous acoustic emission (SAE) conditions found for a van der Waals gas [J.W. Bates and D.C. Montgomery, Phys. Rev. Let. 84, 1180 (2000)], we find that cylindrical and spherical expanding shocks become literally unstable for sufficiently high mode numbers. Counter-intuitively, the effect of exothermicity or endothermicity across the shock is found to be stabilizing or destabilizing, respectively.

I. INTRODUCTION

The studies of shock compression and shock-front stability started simultaneously in the 1940s within nuclear weapons projects. Notwithstanding the impressive progress made in both fields since then, the fundamental shock-front instability theoretically discovered by D'yakov (1954)[1] and Kontorovich (1957)[2] (DK) still challenges the understanding of shock compression, since the associated unstable range typically lies outside the conventional gas dynamics realm. DK instability, which refers to constant-amplitude oscillations of an isolated planar shock, is more likely to be found in non-ideal equations of state (EoS)[3–7] or shocks undergoing modifications in the molecular structure[8–12]. These two different conditions may not necessarily occur separately, as discussed below.

The shocks employed in high-energy-density-physics (HEDP), like those associated with ICF experiments, are extremely intense because achieving the desired compression ratio that fuel ignition calls for pressures and temperatures of the order up to Gbar and a few Kev, respectively. When the matter is compressed to such extreme conditions, the perfect gas EoS does not apply. Sufficiently strong shocks may trigger inelastic processes that ultimately translate into changes in the fluid structure across the shock front. Some examples are phase changes[13,14] that mainly affect inter-atomic forces and/or internal transformations through processes such as dissociation and ionization of gases or ionization of electronic shells in condensed materials, among others[8–11,15–20]. Then, any shock-front stability theory that aims to emulate HEDP conditions needs to account for real fluid EoS, potential endothermicity/exothermicity effects across the shock, and realistic boundary conditions that ensure the shock steadiness.

Shock waves in real fluids have been extensively studied since the theoretical framework of shock propagation was put at disposal by Rankine[21] and Hugoniot[22,23]. They extended the Riemann problem by consistently coupling the conservation equations across the shock, which demanded incorporating the laws of thermodynamics - the specification of the equation of state and the fluid internal energy- that were available at that time. The field has advanced with the progress in the modelization of real fluid EoS, from first-principle theories to practical wide-range approximations such as SESAME[24]. The work of Bethe on the shock theory for an arbitrary equation of state[25], firstly published in 1942, is a distinguished example. Further samples of similar importance were carried out at the same time in the USSR, for which Zel'dovich and Raizer[26] offer a complete compendium and discussion. More up-to-date monographs on the EoS are Refs.[27–30], which contain both experimental and theoretical studies. A review of laboratory and underground shock-compressibility experiments at shock pressures up to hundreds of Mbar is found in Ref.[31]. The platform for EoS studies in the Gbar range developed on the National Ignition Facility (NIF) and some recent experimental results are described in Refs.[32–34].

One broadly used EoS that is suitable to different shock-problem contexts is the van der Waals (vdW) model, since it incorporates effects associated with intermolecular attraction and finite volume by the gas particles[35,36]. Besides, it corresponds to the simplest model that can emulate a phase transition[37,38]. The vdW model is the earliest known non-ideal EoS. It was phenomenologically derived long before the classified work by Bethe, Zel'dovich, and Al'tshuler in the 1940s-1950s. More specifically, at the time between the publication of

[a)] Electronic mail: chuete@ing.uc3m.es

Rankine's[21] and Hugoniot's[22,23] pioneering works, when the concept of a shock wave was novel and not well understood. We refer to van der Waals' 1873 Ph.D. thesis, available in English since 2004[39]. The vdW EoS encodes enough complex physics to provide an example of the DK-unstable shock loading conditions. This was not realized when D'yakov and Landau did their pioneering research on shock stability[1,40], and only discovered by Bates and Montgomery[3] nearly 40 years later. As a reminder, the vdW EoS $p(\rho, T)$ and the corresponding internal energy $E(\rho, T)$ read as

$$p = \frac{\rho R_g T}{1 - b\rho} - a\rho^2 \quad \text{and} \quad E = \frac{R_g T}{\gamma - 1} - a\rho, \qquad (1)$$

where p, ρ and T are the gas pressure, density and temperature variables, respectively, while R_g and γ denote the gas constant and adiabatic index, respectively. With respect to the ideal gas EoS, the term involving the constant a corrects for intermolecular attraction, while b represents the volume occupied by the gas particles (covolume). It is readily seen that (1) reduces to the ideal gas model when a and b approach zero, namely $p = \rho R_g T$ and $E = R_g T/(\gamma - 1)$.

Modifications of the vdW EoS to cover wider conditions have been proposed, such as denser state of matter[41] or hydrocarbons and polar gases, the latter typically modelled through a semi-empirical correction of the vdW EoS[42]. Other modifications are indeed simplifications that, for example, neglect the inter-molecular attraction effect $a = 0$. In that particular case, the vdW EoS turns out to be a reduced Mie-Grüneisen type, where pressure is proportional to specific internal energy with a coefficient that can be an arbitrary function of density. It is usually written as $p = \Gamma(\rho)\rho E$, where $\Gamma(\rho)$ is the Grüneisen coefficient that depends on the density only. For example, for a vdW EoS with $a = 0$, the Grüneisen coefficient reduces to $\Gamma(\rho) = (\gamma - 1)(1 - b\rho)$, while for an ideal gas EoS $\Gamma = \gamma - 1$ is constant.

Canonical shock problems in gas dynamics, such as Guderley-type converging shock, impulsive-loading, or the popular blast wave problem[43–46], can be formulated in absence of temporal and spatial scales through the combination of the inviscid Euler equations and the Rankine-Hugoniot (RH) equations at the shock, provided that additional boundary and initial conditions do not involve spatio-temporal scales. In that case, the possibility of writing a solution in terms of self-similar variables only relies on properties of EoS. That is, there exist constraints in the EoS for the problem to admit a self-similar solution. This was already commented by Sedov, in the third Russian edition of his book[46] in 1954, when discussing the problem of an intense explosion (chapter 4). Sedov quotes Ref.[47], which seems to be the first publication to establish that an EoS compatible with self-similarity allows for a functional (not complete) arbitrariness; to be precise, involving two arbitrary functions relating the pressure with temperature and density. Sedov noted that this was not a general case of a non-ideal EoS: "many interesting EoS (for example vdW EoS) cannot be written" in the form consistent with self-similarity. Axford[48] arrived at a similar conclusion using the mathematical formalism of Lie-group analysis, a theory that was firstly developed and applied to compressible Euler equations by Ovsiannikov[49] . The constraints on the EoS are consequence of the hyperbolic system of nonlinear PDEs that govern the flow field in Guderley-type, blast-wave or impulsive-loading problems.

For blast-wave, impulsive-loading and converging-shock, the condition for self-similarity is that the EoS is of reduced Mie-Grüneisen type, $p = \Gamma(\rho)\rho E$, as satisfied in the vdW EoS with $a = 0$. This property was exploited by Wu and Roberts[50,51], who studied the self-similar solution of the converging-shock with the motivation of understanding the gas bubble collapse at regimes where the density of the air was of the same order of the density of the surrounding liquid, which calls into question the use of an ideal gas EoS. Further examples of self-similar solutions with a simplified vdW EoS can be found in Refs.[52–57]. By way of contrast, the steadiness and uniformity that characterize the flow behind the shock in the generalized Noh problem does not impose such a restriction in the compatibility of the EoS, and a self-similar solution can be constructed for an arbitrary EoS[58,59], and an arbitrary energy addition/subtraction across the shock, as shown in this work. This exception is possible when the scales of density and velocity are time-independent, which is the case for the family of generalized Noh solutions.

The Noh problem configuration is not only interesting because of the high admissibility of the EoS form. Stagnation shocks appear in a wide variety of scenarios. For example, a planar stagnation shock develops when a flyer plate hits a sample[26]. In ICF, planar laser-accelerated foils hit stationary targets to produce x-ray bursts for diagnostic purposes[60] or thermonuclear neutrons[61]. Spherically imploding flows are produced in ICF configurations[62,63], where the stagnation of a low-density fuel via the accretion shock front expanding from the centre of an imploded capsule, back into the converging once-shocked deuterium-tritium plasma, constitutes the first stage of the central hot spot's compression and heating. Fast Z pinches[64–66] implode cylindrically to produce keV x-rays or neutrons[67]. It has been argued[68] that most of the x-ray and neutron yields from Z pinches are generated during the stagnation of magnetically driven, cylindrically imploded mass via an expanding accretion shock. In what concerns the flow dynamics, the steadiness of the post-shock flow associated with the constant velocity of the expanding shock allows doing a justified parallelism with the piston-driven planar shock problem, as demonstrated for inert shocks in Refs.[59,69]. However, experiments in HEDP are seldom exempt of perturbations, particularly so in expanding shock configurations where the shock is formed in an infinitesimal volume. The dynamics of the perturbed flow can completely change the macroscopic picture of the flow field if the shock is

found to be unstable, that ultimately translates into a reduction in the shock compression efficiency.

In this work, we extend the generalized Noh problem and the associated stability analysis to conditions where stagnation enthalpy (defined by the sum thermal enthalpy plus kinetic energy) is not conserved across the shock due to endothermic or exothermic processes induced by shock compression and heating. Formally, one can incorporate the corresponding change of enthalpy into the equation of state, at least for endothermic processes, such as dissociation or ionization. Here, we follow the traditions established in the literature on shock Rankine-Hugoniot's relations with ionization chemistry[19] and on detonation[70–73], explicitly writing up the latent energy absorbed or released in the shock transition. We are interested specifically in the effect of this addition on the stability of a steadily expanding shock front. Recall that the post-shock pressure reduction due to the loss of thermal energy on endothermic processes, such as ionization, increases the shock density compression. Conversely, the compression is reduced by releasing latent heat in exothermic reactions. Exothermic and endothermic reactions can be regarded as increasing and decreasing, respectively, the effective adiabatic exponent γ of the shocked material. Expanding blast waves in an ideal gas are unstable at sufficiently low γ. This is demonstrated in extensive literature on the Vishniac instability of blast waves, which, without support, decay as they propagate[74–79]. However, we focus on steady, supported shock fronts, which are stable for an arbitrary γ in an ideal gas. Therefore, the inclusion of exothermic and endothermic effects is of particular interest for fluids modeled with the vdW EoS, which allows for the DK instability of a steadily expanding shock front[59]. One can establish and quantify stabilizing and destabilizing effects of exothermic and endothermic reactions, which is done below.

A linear small-amplitude stability analysis is employed in this work, as done in Ref.[69] for strong shock in an ideal gas and in Ref.[59] for an arbitrary adiabatic shock. It covers the general case of three-dimensional (3-D) perturbations of the classic Noh solution for spherical geometry, with small-amplitude distortion of the expanding shock front proportional to the spherical harmonic, $\sim Y_l^m(\theta,\varphi)$, and a special case of two-dimensional (2-D) filamentation perturbations, $\sim \exp(\mathrm{i}m\varphi)$, for a cylindrical geometry. The general case of 3-D perturbations in cylindrical geometry, however, needs to be studied separately, as the external arbitrary length scale associated with the axial coordinate impedes the use of separation of variables with the self-similar and temporal coordinates. For the above two scale-free cases, our perturbation problem is solved analytically for an arbitrary EoS, arbitrary shock strength, and energy addition/subtraction. For both spherical and cylindrical cases, the stagnation via a constant-velocity expanding accretion shock wave turns out to be stable when low mode numbers are considered for either an ideal gas and a vdW EoS, and for endo- and exothermic conditions. Then, the distortion amplitude of the expanding shock front decreases as a power of time, with the decay rate being a function of the shock properties and perturbation wavenumber. On the other hand, sufficiently large wavenumbers may lead to an unstable behaviour in the same conditions as those used in Ref.[3] for planar shocks: shocks moving in a vdW gas with low adiabatic index γ. In an ideal gas with the same value of γ, the shock wave is stable for any wavenumber. The factors specific to expanding shock flow, such as its divergence and the non-uniformity of the pre-shock profiles, do not affect the stability criteria in this limit, although the former has an important stabilizing contribution with finite mode numbers. Within the unstable range known for vdW gases, the effect of exothermicity is to reduce the unstable range. By way of contrast, the effect of endothermicity, more likely to occur within the HEDP context, widens the unstable range and can split it into two different regions.

The paper is structured as follows. A review of the asymptotic stability theory for planar isolated shocks is given in section II, where the resemblance and dissimilarity with the generalized Noh problem is analyzed. The case of spontaneous acoustic emission (SAE) is extended to a non-adiabatic shock moving in a vdW gas. In Sec. III it is presented the base flow solution and the first-order perturbation analysis of the Noh reactive problem in the limit of infinitely thin shocks. The eigenvalue patterns are displayed in Sec. IV for different degrees of endothermicity and exothermicity and the radial and transverse limits are analytically evaluated. The stability limits are computed in Sec. V. Lastly, conclusions are given in section VI.

II. ASYMPTOTIC THEORY FOR PLANAR SHOCKS

A. Stability limits

In order to study the stability of the shock wave in a manner that results can be attributed to the shock itself, the shock front must be steady and the downstream flow must be constant. The former ensures that perturbed shock dynamics does not compare to the characteristic time associated with the perturbation-free shock evolution and the latter implies that acoustic perturbations in the post-shock gas are not distorted by the non-uniformness of the flow. Steady shocks can exist if there is a supporting mechanism that maintains downstream pressure constant. If the shock front is over-supported, it is followed by a compression wave that gradually increases its strength, as occurs in Guderley-type converging shocks[43]. By contrast, if the shock is under-supported because it is followed by an expansion wave, its intensity gradually diminishes, as found in Sedov-type blast waves[44,46]. The flow associated with these two cases can be unstable even when the shock front *per se* is surely stable (blast wave[76,77,80] and converging shock[81,82] in an

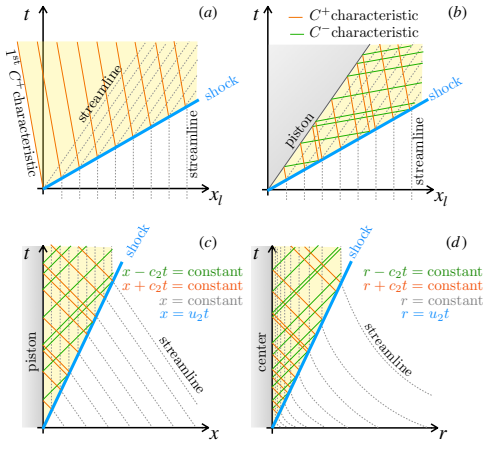

FIG. 1. Fluid particles trajectories and characteristics for an isolated (a) and piston-driven planar shocks (b) in the laboratory reference frame, piston-driven (c) and expanding steady shocks (d) in the compressed gas reference frame.

ideal gas are examples).

For a planar shock, the steady state can be simply given, but not uniquely, by the consideration of a rigid piston that moves at constant speed and keeps downstream pressure constant. For expanding shocks, the supporting mechanism needs for constant energy and momentum entrainment by the converging upstream flow[46,52,58,59]. It maintains the shock in steady state by compensating the expected intensity decay that would occur otherwise. Namely, it is the self-similar characters of the upstream flow what keeps constant the shock intensity, thereby leaving invariant the shock jump conditions and, ultimately, the properties of the shocked gas downstream. We can conclude that investigating the stability of a steady planar shock demands the consideration of the supporting mechanism, a fact that can be qualitatively explained with the aid of the sketches in Fig. 1.

Consider first the case of the isolated shock front moving with velocity u_1 with respect to the stagnant upstream gas, as depicted in Fig. 1 (a). The shock moves with velocity u_2 with respect to the compressed gas, which moves with velocity $u_1 - u_2$ relative to the upstream gas (laboratory) reference frame (x_l, t). Then, the upstream and downstream Mach numbers in the shock-stationary reference frame satisfy $\mathcal{M}_1 = u_1/c_1 > 1$ (supersonic upstream) and $\mathcal{M}_2 = u_2/c_2 < 1$ (subsonic downstream), where c is the corresponding speed of sound. If the shock shape is weakly distorted with a given wavelength, say $\lambda = 2\pi/k$ at $t = 0$, the shock will oscillate with a given oscillation frequency, say ω_s, that scales with $c_2 k$, where c_2 is the speed of sound downstream. This length is considered in the separation of streamlines in Fig. 1 (a). There, upstream and downstream streamlines (C^0 characteristics) are given by $x_l =$ constant and $x_l = (u_1 - u_2)t$+constant, respectively. To compute the transient evolution of the shock front, the linearized Euler equations must be integrated within the domain enclosed by the shock front and the leading acoustic wave radiated at $t = 0^+$, given by $x_l = u_1 t$ and $x_l = (c_2 - u_1 + u_2)t$ in the laboratory reference frame, respectively. It is in this isolated-shock condition where the classical DK stability analysis applies.

The stability conditions for a steady isolated shock wave can be written in terms of the DK parameter

$$h = \frac{p_2 - p_1}{V_1 - V_2}\left(\frac{\mathrm{d}V_2}{\mathrm{d}p_2}\right)_H = -u_2^2\left(\frac{\partial \rho_2}{\partial p_2}\right)_H \qquad (2)$$

that measures the slope of the Hugoniot curve relative to the Rayleigh-Michelson line on the (V, p) plane. Here p, ρ, $V = 1/\rho$, and u denote the pressure, density, specific volume, and fluid velocity with respect to the shock front, respectively, subscripts 1 and 2 refer to pre- and post-shock states, and the derivatives are calculated along the Hugoniot curve with the pre-shock pressure and density fixed. For an isolated steady planar shock front, the classic stability theory predicts an oscillatory decay of perturbations as $t^{-3/2}$ ($t^{-1/2}$ in the strong-shock limit), with a constant oscillation frequency, for any wavenumber and any EoS[11,83,84], provided that the parameter h is in the stable range, $-1 < h < h_c$, where

$$h_c = \frac{1 - \mathcal{M}_2^2(1 + \mathcal{R})}{1 - \mathcal{M}_2^2(1 - \mathcal{R})}, \qquad (3)$$

and $\mathcal{R} = \rho_2/\rho_1$ is the shock density compression ratio. For $h_c < h < 1 + 2\mathcal{M}_2$, shock perturbations with certain wavevectors oscillate at constant amplitude, causing spontaneous acoustic emission (SAE) from the shock front[2,30,85,86]. Absolutely unstable ranges are $h < -1$ and $h > 1 + 2\mathcal{M}_2$, for which the exponential growth of shock-front perturbations is associated with conditions that render multi-valued[87,88] or multi-wave[89,90] solutions of the planar Riemann/piston problem. For a non-reactive shock moving in an ideal gas $h = -1/\mathcal{M}_1^2$, $h_c = -1/(2\mathcal{M}_1^2 - 1)$, so that the stability condition $-1 < h < h_c$ is always satisfied.

Now consider the presence of a rigid piston supporting the shock, as sketched in Fig. 1 (b). The integration domain reduces to the region enclosed by the shock $x_l = u_1 t$ and the moving piston $x_l = (u_1 - u_2)t$. In such case, the radiated acoustic waves reverberate, thereby involving additional frequencies to the oscillating shock dynamics. It is readily seen that the reflected waves associated with C^- characteristics (green color) arrive at the shock with a lower frequency by the Doppler shift effect. The trajectories of the two family of characteristics in the laboratory reference frame are straight lines because

of the uniformity of the flow, namely:

$$C^0: \quad \frac{\mathrm{d}x_l}{\mathrm{d}t} = u_1 - u_2, \tag{4a}$$

$$C^\pm: \quad \frac{\mathrm{d}x_l}{\mathrm{d}t} = u_1 - u_2 \pm c_2. \tag{4b}$$

In the stable range, $-1 < h < h_c$, the acoustic disturbances decay exponentially with the distance from the shock, which implies that the acoustic coupling is very weak, even for short periods of time close to $t = 0$. This is the reason why stability threshold and the decay rate of the shock oscillations amplitude in the stable range takes the same form in both isolated and piston-driven configurations[91–93]. Likewise, the absolutely unstable ranges $h < -1$ and $h > 1 + 2\mathcal{M}_2$, which are exclusively associated with the RH curve, are the same regardless the boundary condition. By way of contrast, including a supporting mechanism can make a difference in the marginally stable/SAE range, $h_c < h < 1 + 2\mathcal{M}_2$, since the acoustic radiation does not decay with the distance from the shock and the acoustic coupling is always present. As noted in Refs.[88,93], the amplitude of a reverberating acoustic wave grows as a power of time for $h > 1$ when perturbations are one-dimensional. For two-dimensional perturbations, the stability analysis in Ref.[94] for $h_c < h < 1 - 2\mathcal{M}_2^2$ did not find any qualitative distinctness in the shock front perturbation behavior when a piston is involved. On the other hand, Ref.[95] found instability, a linear growth of shock perturbations in the whole range $h > h_c$. Then, there is no clear consensus about the shock dynamics in the marginally stable/SAE range.

A spherically or cylindrically expanding shock front, just like a planar one, can be steady if a constant-velocity inflow of incident mass supports it. In such case, the center or axis of symmetry plays the role of the rigid piston and the shock strength, characterized by velocity, pressure and density jumps across the shock, is time independent, thereby yielding uniform properties of the shocked gas put at rest. See Fig. 1 (c) and (d). Such an expanding accretion-shock flow is described by a self-similar solution of ideal compressible fluid dynamics equations, which exists for an arbitrary EoS of the fluid and the parameters of the incident flow[11,58]. While the streamlines in Fig. 1 (a)-(c) are uniformly separated, with the spacing indicated the characteristic perturbation length being inversely proportional to the shock oscillation frequency, the streamlines in Fig. 1 (d) are not equidistant. The consideration of a length-free problem impedes the association of the shock dynamics to a single characteristic length and the divergence effect by the expanding shock decreases the frequency of the associated perturbations at a given location with time.

However, the Noh's problem owns the main properties as the piston-driven shock. The post-shock gas is characterized by straight streamlines, where the fluid particles are put at rest and by acoustic waves that move at the speed of sound c_2. They can be written in terms of characteristics through

$$C^0: \quad \left.\frac{\mathrm{d}x}{\mathrm{d}t}\right|_{\text{planar}} = \left.\frac{\mathrm{d}r}{\mathrm{d}t}\right|_{\text{expanding}} = 0, \tag{5a}$$

$$C^\pm: \quad \left.\frac{\mathrm{d}x}{\mathrm{d}t}\right|_{\text{planar}} = \left.\frac{\mathrm{d}r}{\mathrm{d}t}\right|_{\text{expanding}} = \pm c_2. \tag{5b}$$

It must be noticed that, although following the same trajectories, the amplitude of the sonic perturbations is affected by the divergent flow configuration, which will be found to exert a stabilizing effect. In addition, the extension to multidimensional perturbations, either in planar, cylindrical or spherical geometries, does also modify the acoustic field. This is because, unlike one-dimensional acoustic waves, two- or three-dimensional acoustic fronts radiated from the shock can be evanescent waves if the shock oscillation frequency is not sufficiently high.

B. Application to a reactive shock in a vdW gas

1. *Rankine-Hugoniot equations*

According to equations (2) and (3), the DK stability boundary for a planar shock depends on three parameters: the shock compression ratio $\mathcal{R}$, the post-shock Mach number $\mathcal{M}_2$ and the slope of the RH curve through the parameter h. The first two can be constructed by integrating the conservation equations across the shock. In particular, if we admit the possibility of having exothermic or endothermic effects throughout the shock wave, the corresponding mass, streamwise momentum and energy conservation equations read as

$$\rho_1 u_1 = \rho_2 u_2, \tag{6a}$$

$$p_1 + \rho_1 u_1^2 = p_2 + \rho_2 u_2^2, \tag{6b}$$

$$\frac{p_1}{\rho_1} + E_1 + \frac{u_1^2}{2} + q = \frac{p_2}{\rho_2} + E_2 + \frac{u_2^2}{2}, \tag{6c}$$

where p is the thermal pressure, E is the internal energy and q measures the energy removed ($q < 0$) or released ($q > 0$) per unit mass by the corresponding process undergoing across the shock. To solve the RH equations, it proves convenient to write the internal energy as a function of p and ρ by direct combination of the two relationships in (1), namely

$$E = \frac{(p + \rho^2 a)(1 - b\rho)}{\rho(\gamma - 1)} - a\rho. \tag{7}$$

Likewise, the speed of sound is written as a function of pressure and density

$$c^2 = \frac{\gamma(p + \rho^2 a)}{\rho(1 - b\rho)} - 2a\rho. \tag{8}$$

Simple manipulation of (8) provides $c^2 = \gamma R_g T = \gamma p/\rho$ as the square of the speed of sound for an ideal gas $a = b = 0$.

Equations (6)-(8) suffice to provide the shock jump properties in steady state, upon condition that the non-equilibrium inner structure, where endothermic or exothermic processes undergo, has no influence in the shock beyond the net energy factor q, assumed constant. This condition can be regarded as a twofold restriction: the inner structure must be stable and the net energy change cannot depend on the shocked gas properties. The latter is effectively satisfied in the most common exothermic shock configuration, a gaseous detonation, since the combustion process, once initiated, progresses until fuel depletion releasing all potential chemical energy. Only in some particular conditions, mostly associated with rich mixtures, products depend on equilibrium conditions downstream. Then, the variation of q with the Mach number affects the shock dynamics, and therefore, modify shock stability properties[11,12]. For the utmost practical applications, q can be regarded as a constant parameter in gaseous detonations. As a matter of example, in q is of the order of 10^6 J/kg in stoichiometric reactive mixtures made of air and light hydrocarbons, and $p_1/\rho_1 \sim 10^5$ J/kg in normal conditions. We conveniently define the dimensionless energy factor as $\mathcal{Q} = q\rho_1/p_1$ that indicates the heat release relative to the thermal specific energy, which yields $\mathcal{Q} \sim 10$. This renders propagation Mach numbers of the order of 10 in a self-sustained detonation, termed Chapman-Jouget (CJ) in the combustion argot. The CJ condition corresponds to the maximum value of heat release for a given propagation Mach number, although much smaller values of $\mathcal{Q}$ for the same shock intensity can be obtained in diluted mixtures, on condition that an external mechanisms contributes in supporting the exothermic shocks. The assumption on the inner structure stability is harder to meet in gaseous detonations, unless it is sufficiently overdriven (externally supported), i.e., the propagation shock Mach number is significantly higher than that associated with the CJ condition. Equivalently, this condition imposes the value of $\mathcal{Q}$ to be sufficiently low compared with the associated CJ value for a given propagation Mach number. We anticipate that the interest values for which the shock turns unstable to self-induced acoustic disturbances (not generated in the inner reaction region) is $\mathcal{Q} \sim 1$, which is one order of magnitude smaller to that found in inherently unstable CJ detonations.

For exothermic shocks, we limit ourselves to the case of overdriven detonations, i.e., the upstream and downstream Mach numbers satisfy $\mathcal{M}_1 > 1$ and $\mathcal{M}_2 < 1$, respectively. Note that the CJ limit $\mathcal{M}_2 \to 1$ can only be approached asymptotically if the whole supersonic front is considered a discontinuity. Notice also that $\mathcal{M}_2 > 1$ (underdriven) is actually feasible, but it requires an additional mechanism to support a propagating reactive front: radiation transport, as in so-called Marshak waves[96] or in laser-supported detonations[97]. Reaction fronts of this kind require one boundary condition additional to (6) and will not be considered here. The possibility of considering exothermic waves with $\mathcal{M}_1 < 1$, typically deflagrations, also demands the specification of additional information -the reaction rate and the associated transport mechanisms for heat and species- and they are not considered in this analysis.

For endothermic transformations, the instability associated with the non-equilibrium inner region is seldom expected, but the energy taken from the fluid particles may likely depend on the post-shock conditions, e.g., shocks triggering molecular excitation, dissociation, ionization or phase change[8,9,19]. A recurrent example is related to shocks involved in hypersonic flight[98]. The endothermic processes are dictated by the type of molecular structure, which can be simplified to molecular oxygen and nitrogen in case of considering atmospheric air as the flight medium. The characteristic vibrational temperatures of O_2 and N_2 are of the order of 10^3 K, which is relatively feasible to reach at the hypersonic boundary $\mathcal{M}_1 \sim 5$ as the temperature jump is roughly proportional to $\mathcal{M}_1^2$ in ideal gases. When the shock strengthens, the associated endothermic effects of dissociation and ionization enter into play. Although their characteristic temperatures are of the order of 10^4-10^5 K, their functional dependence with temperature makes these effects noticeable at much lower temperatures. The main characteristic of the RH curve associated with these effects is the turning point at the highest compression ratio (see Fig. 2 in Ref.[99]). Further examples closer to HEDP, which may include radiative shocks, also exhibit turning points in the RH curve, as computed in Ref.[19]. That said, assuming constant the value of $\mathcal{Q} < 0$ is not a marginal situation since many of the above-mentioned phenomena saturate at some shock intensity. As mentioned above, the value at which the instability threshold is found is relatively small $-\mathcal{Q} \sim 1$, considering q a constant parameter indirectly imposes low concentration of the active species undergoing molecular transformations.

Then, as a first approximation, we restrict ourselves to energy variations that are not effectively sensitive with the shock conditions:

$$\frac{\partial \mathcal{Q}}{\partial \mathcal{M}_1} \ll \frac{1}{E_1}\frac{\partial E_2}{\partial \mathcal{M}_1} \sim \frac{1}{E_1}\frac{\partial u_2^2}{\partial \mathcal{M}_1}, \tag{9}$$

thus, $\mathcal{Q} =$ constant, with $\mathcal{Q}$ being a free parameter with some constraints. Notice that in case of considering $\mathcal{Q}$ a variable function, an additional equation should be included to model the dependence of $\mathcal{Q}$ with post-shock properties. In our case, the problem formulation of the jump conditions across the shock is closed with equations (6a)-(6c) and (7), provided that upstream conditions are known and an additional input related to the supporting mechanism is specified, typically the propagation shock Mach number $\mathcal{M}_1$.

To compute the jump conditions, the dimensionless constants for the constitutive parameters of the EoS are reduced with pre-shock conditions, i.e., $\alpha_1 = a\rho_1^2/p_1$ and $\beta_1 = b\rho_1$. Thus, the RH curve $\mathcal{P}(\mathcal{R})$ involves four the dimensionless constants associated with the gas properties $\{\gamma, \mathcal{Q}, \alpha_1, \beta_1\}$, specifically

$$\mathcal{P} = \frac{\mathcal{R}\left[\gamma + 1 - 2\beta_1(\alpha_1 + 1) - 2\alpha_1(\gamma - 2)\right] - (\gamma - 1) + 2\alpha_1\mathcal{R}^2\left(\gamma - 2 + \beta_1\mathcal{R}\right) - 2\mathcal{Q}\mathcal{R}(\gamma - 1)}{(\gamma + 1) - \mathcal{R}\left(\gamma - 1 + 2\beta_1\right)}. \tag{10}$$

The dependence of post-shock flow with the shock strength can be obtained with the aid of the Rayleigh-Michelson relationships

$$\mathcal{P} = 1 + \gamma_{1s}\mathcal{M}_1^2\left(1 - \mathcal{R}^{-1}\right) \tag{11}$$

obtained from direct combination of mass and momentum conservation equations (so $\mathcal{Q}$ does not appear explicitly), where the definition of the effective sonic constant is conveniently introduced

$$\gamma_{1s} = \frac{\rho_1 c_1^2}{p_{1s}} = \gamma\frac{1 + \alpha_1}{1 - \beta_1} - 2\alpha_1. \tag{12}$$

The post-shock Mach number reads as

$$\mathcal{M}_2 = \frac{\mathcal{M}_1}{\sqrt{\mathcal{R}}}\sqrt{\frac{\gamma_{1s}(1 - \beta_1\mathcal{R})}{\gamma\left(\mathcal{P} + \alpha_1\mathcal{R}^2\right) - 2\alpha_1\mathcal{R}^2(1 - \beta_1\mathcal{R})}}. \tag{13}$$

It is immediate to see that for $\mathcal{Q} = \alpha_1 = \beta_1 = 0$, the sonic constant $\gamma_{1s} = \gamma$, which ultimately renders

$$\mathcal{P} = \frac{\mathcal{R}\left(\gamma + 1\right) - \left(\gamma - 1\right)}{\left(\gamma + 1\right) - \mathcal{R}\left(\gamma - 1\right)}, \tag{14a}$$

$$\mathcal{R} = \frac{(\gamma + 1)\mathcal{M}_1^2}{2 + (\gamma - 1)\mathcal{M}_1^2}, \tag{14b}$$

$$\mathcal{M}_2^2 = \frac{(\gamma - 1)\mathcal{M}_1^2 + 2}{2\gamma\mathcal{M}_1^2 - \gamma + 1}, \tag{14c}$$

for the non-reactive Rankine-Hugoniot equation, mass compression ratio and post-shock Mach number, for an ideal equation of state. For such case, only compressive shocks are admissible: they exist and are stable. On the other hand, vdW EoS may yield compressive shocks, as well as rarefaction shocks (also called negative shocks, where density downstream is lower than density upstream), even for $\mathcal{Q} = 0$. They may be either admissible or inadmissible depending on the EoS and shock properties[25,37,100,101]. We restrict the analysis to conditions that render uniqueness in the Riemann problem solution and the only solution corresponds to a compressive shock: the RH curve, as shown in Fig. 2 is monotonic ($h < 0$). The above mentioned studies on the admissibility of shock types in vdW gases do not consider energy variations across the shock. To the authors knowledge, this is the first time a shock wave in a vdW gas is analytically evaluated in a reactive scenario, thereby justifying a brief description, offered below, of the base-flow properties given by the RH equations.

In our case, we take the energy factor $\mathcal{Q}$ as a free parameter that is bounded in both negative (endothermic) and positive (exothermic) cases. This is readily seen if we picture the non-adiabatic shock as the sum of the precursor adiabatic shock ($\mathcal{Q} = 0$) plus the associated

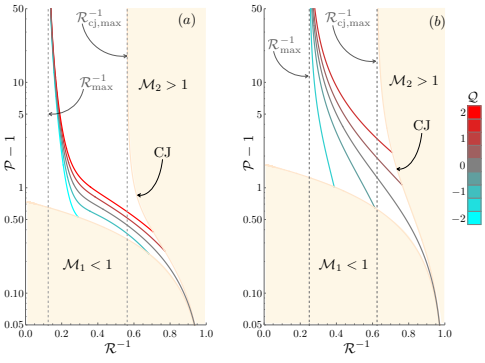

FIG. 2. Reactive Rankine-Hugoniot curve for a vdW gas with $\gamma = 31/30$, $\alpha = 1/2$, and $\beta = 1/9$ (a) and for an ideal gas with $\gamma = 5/3$ (b) for different degrees of exothermicity and endothermicity.

non-equilibrium zone. The properties right behind the former are just given by (10)-(13), provided that $\mathcal{Q} = 0$. Then, the compressed gas evolves differently depending on the particular phenomena. For $\mathcal{Q} < 0$, the endothermic cooling effect increases the gas density with the corresponding flow velocity reduction (measured from the shock front). The largest negative value of $\mathcal{Q}$ is that given by the sonic condition upstream $\mathcal{M}_1 \to 1$. On the other side, for exothermic shocks, the reactive process increases the temperature of the gas that expands. The maximum value of $\mathcal{Q}$ is that given by the sonic condition downstream $\mathcal{M}_2 \to 1$, the CJ condition.

The value of the maximum energy delivered for a given shock condition can be written analytically for a vdW EoS as a function of the mass compression ratio, namely

$$\begin{aligned}\mathcal{Q}_{\rm max} = \frac{(\mathcal{R} - 1)^2}{2(\gamma - 1)\mathcal{R}\left[\mathcal{R}(\beta_1 + \gamma) - (\gamma + 1)\right]}\big[&-\gamma(\gamma + 1) \\ &+ 2\alpha_1\beta_1\mathcal{R}^3(2\beta_1 + \gamma - 1) + \alpha_1\mathcal{R}^2\left(2(\beta_1 - 4)\beta_1\right. \\ &+ \left.(\gamma - 2)(\gamma - 1)\right) - 2\alpha_1(\gamma + 1)\mathcal{R}(\beta_1 + \gamma - 2)\big]\end{aligned} \tag{15}$$

which reduces to

$$\mathcal{Q}_{\rm max} = \frac{\gamma(\gamma + 1)(\mathcal{R} - 1)^2}{2(\gamma - 1)\mathcal{R}\left[\mathcal{R}\gamma - (\gamma + 1)\right]} \tag{16}$$

for an ideal gas EoS. Notice that not all values of $\mathcal{R}$ are possible when sonic conditions apply downstream.

By substitution of (15) into (10), we obtain the curves $\mathcal{P}(\mathcal{R}^{-1})$ plotted in Fig. 2 corresponding to CJ conditions. The shadowed region above this curve (top right side) corresponds to underdriven detonations, excluded in the

analysis because the possibility of having $\mathcal{M}_2 > 1$ cannot be exclusively determined by (6a)-(6c). It is also found that, within the CJ condition, the maximum compression ratio for a vdW EoS is

$$\mathcal{R}_{\mathrm{cj,max}} = \frac{\gamma+1}{\gamma+\beta_1}, \tag{17}$$

that corresponds to the strong-shock limit for a self-sustained detonation. If we admit overdrive, i.e., if pressure downstream is also exerted by any supporting mechanism downstream, the maximum mass compression ratio across the shock increases to

$$\mathcal{R}_{\mathrm{max}} = \frac{\gamma+1}{\gamma-1+2\beta_1}, \tag{18}$$

that is the value that makes (10) go to infinity. This value does not depend on the heat release since it corresponds to thermal energies downstream that are much larger than the energy factor $\mathcal{Q}$, thereby being the equivalent to that for adiabatic shocks. This limit does not change for $\mathcal{Q} < 0$ so long the endothermic contribution remains invariant with the shock intensity. See dashed lines in Fig. 2.

Likewise, the supersonic condition of the propagating shock imposes $\mathcal{Q}$ to be larger than

$$\begin{aligned}\mathcal{Q}_{\mathrm{min}} = -\frac{(\mathcal{R}-1)^2}{2(\beta_1-1)(\gamma-1)\mathcal{R}^2}\,[&-\gamma(\gamma+1)\\ &+\alpha_1\left(2(\beta_1-1)\mathcal{R}(2\beta_1+\gamma-2)\right.\\ &+\left.2(\beta_1-1)\beta_1\mathcal{R}^2\right)-(\gamma+1)(2\beta_1+\gamma-2)\big],\end{aligned} \tag{19}$$

which gives $\mathcal{Q}_{\mathrm{min}} \leq \mathcal{Q} < \mathcal{Q}_{\mathrm{max}}$ as the possible range of the energy factor. The limiting sonic condition $\mathcal{M}_1 = 1$ for pressure is obtained substituting (19) into (10). We obtain the curves $\mathcal{P}(\mathcal{R}^{-1})$ plotted in Fig. 2, where the region below this curve (bottom left side) is omitted as it corresponds to $\mathcal{M}_1 < 1$.

The Rankine-Hugoniot curves for a vdW gas with $\gamma = 31/30$, $\alpha = 1/2$, and $\beta = 1/9$ (a) and for an ideal gas with $\gamma = 5/3$ (b) are displayed in Fig. 2 for different values of $\mathcal{Q}$. The non-reactive case corresponds to the grey curves that depart from the upstream conditions in the weak shock limit: $\mathcal{P} = 1$ and $\mathcal{R} = 1$. When endothermic effects are considered (blue curves), the departing points (minimum mass compression ratio) shift to the left, corresponding to the sonic condition upstream $\mathcal{M}_1 = 1$. On the other side, when exothermic effects are considered (red curves), the departing points also shift to the left, corresponding to sonic conditions downstream $\mathcal{M}_2 = 1$.

It has been mentioned that a typical value of Q for detonations is of the order of 10. However, it will be noted in this study that $\mathcal{Q}$ of the order of unity are used, as showed in Fig. 3 and Fig. 4. This is because in order to study stability one must be in the region where h exceeds its critical value h_c (regime in which the expected SAE occurs). It is reminded that divergence of the shock provides an additional stabilizing effect, being more restrictive. Any detonation case with a typical $\mathcal{Q}$ higher than those shown will predictably present a stable front, as long as the hypotheses presented apply.

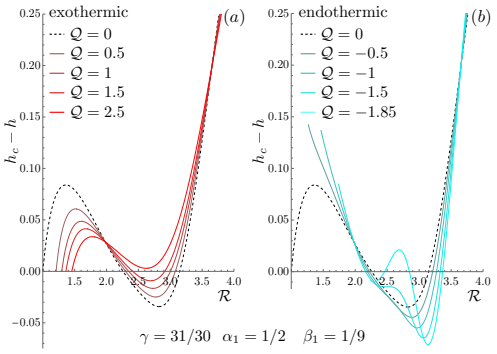

FIG. 3. Stability range $h_c - h$ for a vdW gas with $\gamma = 31/30$, $\alpha_1 = 1/2$, and $\beta_1 = 1/9$ and different degrees of exothermicity (a) and endothermicity (b).

2. The DK instability range for planar shocks

As commented in previous subsection, the stability limits of a planar shock can be expressed in terms of the DK parameter h. For a reactive shock in a vdW gas, this factor can be analytically derived from (2), (10) and (11), through the equation

$$h = -\gamma_{1s}\frac{\mathcal{M}_1^2}{\mathcal{R}^2}\left(\frac{\partial\mathcal{P}}{\partial\mathcal{R}}\right)^{-1}, \tag{20}$$

while h_c is obtained by direct substitution of relationships (10)-(13) in equation (3).

For the pre-shock and vdW EoS parameter values used in Refs.[3,59] for adiabatic shocks, associated with high gas compressibility $\gamma = 31/30$ with $\alpha_1 = 1/2$, and $\beta_1 = 1/9$, the DK instability condition $h > h_c$ is met within an interval of shock strengths corresponding to density compressions $2.2586 < \mathcal{R} < 3.1482$. This is shown in Fig. 3, where the adiabatic curve $h_c - h$ is displayed in dashed line. The effect of exothermicity (a) and endothermicity (b) is also computed in solid orange and cyan colors, respectively. It is found that increasing the exothermic contribution tends to stabilize the shock and so that for $\mathcal{Q} > \mathcal{Q}_c = 2.2285$, the condition $h > h_c$ is never met. By contrast, endothermicity does not exhibit a clear trend. While the range of compression ratios $\mathcal{R}$ at which $h > h_c$ can occur increases, there may exist an inner region where $h < h_c$ for sufficiently endothermic contributions.

The form of the RH curve for the cases displayed in Fig. 3 is that plotted in Fig. 2 in solid lines. For exothermic shocks, the condition $h = -1$ is marginally achieved in the CJ limit, where $\mathcal{M}_2 = 1$, that corresponds to the minimum value of $\mathcal{R}$ in the red curves of Fig. 3 (and the maximum value of $\mathcal{R}^{-1}$ in red curves in Fig. 2). For endothermic shocks, we can see that the RH curve flattens less when $\mathcal{Q} < 0$ for low mass compression ratios, which

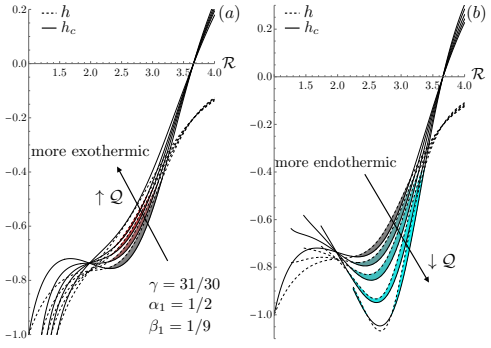

FIG. 4. DK parameters h and h_c for a vdW gas with $\gamma = 31/30$, $\alpha_1 = 1/2$, and $\beta_1 = 1/9$ and different degrees of exothermicity (a) and endothermicity (b), corresponding to those in Fig.3

turns into higher values of h; an effect that occurs with a much weaker intensity in ideal gases (b). Although this explains the increase of h with endothermicity, the instability limits cannot be uniquely determined the by RH shape as it also involves the parameter h_c. As we see in Fig. 4, where both h and h_c parameters are computed separately in the same shock conditions as in Fig. 3, the two functions follow a similar trend in what concerns to variations in $\mathcal{R}$ and $\mathcal{Q}$, yet in some particular conditions h is slightly higher than h_c (shadowed region), thereby providing instability. This subtle property is what impedes us to isolate effects that could explain the lead to the DK instability when varying the degree of endothermicity/exothermicity.

When considering adiabatic shocks, $\mathcal{Q} = 0$, the asymptotic sonic condition downstream $1 - \mathcal{M}_2 \ll 1$ only occurs in the acoustic limit $\mathcal{M}_1 - 1 \ll 1$. Now, as we admit an order-of-unity change in the energy factor, these two limits get decoupled. A distinguished case corresponds to exothermic shocks in the CJ limit, $\mathcal{M}_2 \to 1$, where the Rayleigh-Michelson line, given by (11), is tangent to the Rankine-Hugoniot curve, determined by (10). In other words, $\partial\mathcal{P}/(\partial\mathcal{R})$ in (11) equals the same derivative in (10), thereby making the DK parameter $h = -1$.

On the other hand, the case $\mathcal{M}_1 \to 1$ associated with endothermic shocks does not provide constant values for h and $\mathcal{M}_2$ but rather functions that depend on the shock properties:

$$h(\mathcal{M}_1 \to 1) = -\left[\alpha_1(2\beta_1+\gamma-2)+\gamma\right]\left[-\gamma+\mathcal{R}(2\beta_1+\gamma-1)-1\right]/\big\{\gamma(\gamma+\mathcal{R}(2\beta_1-\gamma-3)+1) + \alpha_1\left[(\gamma+1)(2\beta_1+\gamma-2)+4(\beta_1-1)\beta_1\mathcal{R}^4+2(\beta_1-1)(\gamma-2)\mathcal{R}^3-(\gamma+1)\mathcal{R}(2\beta_1+\gamma-2)\right]\big\} \quad (21)$$

and

$$\mathcal{M}_2(\mathcal{M}_1 \to 1) = \sqrt{\frac{(\beta_1\mathcal{R}-1)(2\alpha_1(\beta_1-1)+(\alpha_1+1)\gamma)}{(\beta_1-1)\gamma\left[\alpha_1\left(\mathcal{R}^3-2\mathcal{R}+2\right)+\mathcal{R}\right]+2\alpha_1(\beta_1-1)\mathcal{R}^3(\beta_1\mathcal{R}-1)-(\alpha_1+1)\gamma^2(\mathcal{R}-1)}} \quad (22)$$

for the DK parameter and the post-shock Mach number, respectively. Exploring the possibility of SAE is readily given by $h - h_c > 0$, where the value of h_c as a function of $\mathcal{R}$ is derived from (3) with use made of (22). Unlike the CJ condition, this limit does not render any condition qualitatively different to an adiabatic shock.

III. LINEAR STABILITY OF THE NOH'S PROBLEM

Previous section has been devoted to the study of the stability of an isolated planar shock, where the energy factor $\mathcal{Q}$ is due to internal processes undergoing across the shock. Besides, only small perturbations have been considered. That is, the thickness of the non-equilibrium region is much smaller than the perturbation transverse wavelength and the displacement of the shock from its planar flat shape is also much smaller than the perturbation wavelength. This warrants the decoupling of the perturbation modes into vortical, entropic and acoustic, upon which the perturbation analysis relies. In our case, either upstream or downstream flow variables are subject to isentropic transformations of acoustic type. The source of irreversible transformations, that will take the form of entropic and vortical spots downstream, are only generated across the shock.

Likewise for the expanding shock problem, the endothermic and exothermic effects triggered by the shock passage are assumed to occur in an infinitesimal thickness region attached to the shock, thereby allowing the reactive shock be treated as a moving discontinuity. As the Noh problem is scale free, there is no externally imposed length affecting the flow dynamics. Accordingly, the equations that govern the flow outside the shock are the linear inviscid non-reactive Euler conservation equations, namely

$$\frac{\partial\rho}{\partial t} + \nabla\cdot(\rho\boldsymbol{v}) = 0, \quad (23)$$

$$\frac{\partial \boldsymbol{v}}{\partial t} + \boldsymbol{v}\cdot\nabla\boldsymbol{v} + \frac{1}{\rho}\nabla p = 0, \tag{24}$$

$$\frac{\partial p}{\partial t} + \boldsymbol{v}\cdot\nabla p = c^2\left(\frac{\partial \rho}{\partial t} + \boldsymbol{v}\cdot\nabla\rho\right), \tag{25}$$

where $\rho(\boldsymbol{x},t)$, $\boldsymbol{v}(\boldsymbol{x},t)$, $p(\boldsymbol{x},t)$ and $c(\boldsymbol{x},t)$ stand for the density, the velocity, the pressure and the speed of sound, respectively, as functions of the Eulerian coordinate $\boldsymbol{x}$ and the time t.

Equations (23) and (24) refer to the conservation of mass and momentum, respectively, while (25) refers to the conservation of entropy of the fluid particles. The speed of sound is related to the isentropic condition associated with the flow perturbations. It can be determined with the aid of the equation of state expressing the specific internal energy as a function of density and pressure $c = c(p,\rho)$, as shown in (8) for the vdW EoS. Note that (25) should be correspondingly modified when finite-rate reaction processes are considered behind the shock, which would call for an additional relationship to describe the reaction progress rate and the net energy released/substracted in the process q. In such case, the shock would be simply described with the corresponding adiabatic Rankine-Hugoniot curve. It is readily seen that finite-rate reaction processes cannot be neglected at the first stage of the shock expansion, where the shock radius is comparable to the reaction region. Then, the case considered in this work reduces to an intermediate asymptotic regime where the shock radius is sufficiently large compared to the reaction region. Regarding the perturbation analysis derived below, an additional condition is that the shock corrugation amplitude must be much smaller than the shock radius, yet much larger than the reaction zone.

A. Generalized Noh problem for reactive shocks

The general Noh problem is formulated as follows. At $t = 0^-$, an infinite space is filled with a uniform material whose density and pressure are denoted by ρ_0 and p_0. Its initial velocity is supersonic, it has the same absolute value v_0 everywhere, and it is directed at each point to the plane, axis, or center of symmetry in the cases of planar, cylindrical, or spherical symmetry, respectively. The 1D accretion-shock flow emerging after $t = 0^+$, maintains its initial planar, cylindrical, or spherical symmetry. We need to determine the preshock profiles of density, pressure, and velocity and calculate the strength of the expanding shock wave and the postshock conditions, for which the integration of (23)-(25) is initiated with

$$\rho_1(r, t=0) = \rho_0, \tag{26a}$$
$$p_1(r, t=0) = p_0, \tag{26b}$$
$$\boldsymbol{v}_1(r, t=0) = -v_0\boldsymbol{e}_r, \tag{26c}$$

where $\boldsymbol{x} = r\boldsymbol{e}_r$ and $\boldsymbol{e}_r$ is a unit vector in the positive radial direction. Subscript 1 refers to variable conditions in the whole domain ahead of the shock front. A sketch of the generalized Noh problem is depicted in Fig.5.

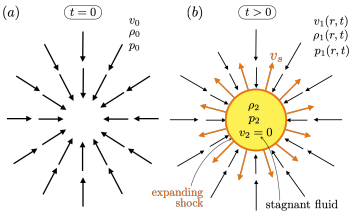

FIG. 5. Sketch of the generalized Noh problem at $t = 0$ (a) and $t > 0$ (b).

The lack of scales justifies the definition of the self-similar coordinate

$$\xi = \frac{r}{v_0 t} \tag{27}$$

to describe the converging flow. By direct substitution in the system of equations (23)-(25), the mass, the radial momentum, and the energy conservation equations are rewritten as a system of differential equations for ξ, namely

$$(v_1 - \xi v_0)\frac{\mathrm{d}\ln\rho_1}{\mathrm{d}\xi} + \frac{\mathrm{d}v_1}{\mathrm{d}\xi} + \frac{(\nu-1)v_1}{\xi} = 0, \tag{28a}$$
$$(v_1 - \xi v_0)\frac{\mathrm{d}v_1}{\mathrm{d}\xi} + \frac{1}{\rho_1}\frac{\mathrm{d}p_1}{\mathrm{d}\xi} = 0, \tag{28b}$$
$$\frac{\mathrm{d}p_1}{\mathrm{d}\xi} - c_1^2\frac{\mathrm{d}\rho_1}{\mathrm{d}\xi} = 0. \tag{28c}$$

The coefficient ν represents the geometry. The case $\nu = 1$ denotes a planar geometry that renders a trivial flat-profile behaviour, and $\nu = 2$ and $\nu = 3$ refer to the cylindrical and spherical geometries, respectively, which provide a variable flow as a result of the inwards mass accumulation.

Equations (28a)-(28c) are supplemented with the equation for the speed of sound $c_1 = c(p_1,\rho_1)$, to be determined with (8), and the associated boundary conditions

$$\frac{v_1(\xi\to\infty)}{v_0} = \frac{\rho_1(\xi\to\infty)}{\rho_0} = \frac{p_1(\xi\to\infty)}{p_0} = 1 \tag{29}$$

that impose the flow properties relatively far from the center at a given time frame $r \gg v_0 t$. Notice that $c_1(\xi\to\infty) = c_0$. However, the integration of (28a)-(28c) does not provide a physically meaningful solution in the whole domain $\xi > 0$. The solution calls for the consideration of an expanding shock that emerges at $t = 0^+$ and puts the downstream flow at rest. The shock moves at constant speed v_s and always encounters the same properties upstream since both shock position and upstream variable rate of change are linearly proportional to t, thereby rendering uniform flow variables downstream.

The velocity of the shock v_s is to be determined, which translates into obtaining the position of the shock in the self-similar coordinate $\xi_s = v_s/v_0$. This can be done with the aid of the RH equations across the shock, (6a)-(6c), where upstream conditions are evaluated at the front position $u_1(\xi_s) = \xi_s v_0 - v_1(\xi_s)$, $\rho_1 = \rho_1(\xi_s)$, $p_1 = p_1(\xi_s)$ and downstream velocity measured at the shock is $u_2 = u_1(\xi_s) - \xi_s v_0$. The endothermic and exothermic processes are assumed to occur within the shock front, thereby not involving any additional scale. In what respect to the resemblance with detonations, notice that the present work omits its direct initiation, which is still an open problem in combustion theory[102,103].

In sum, equations (28a)-(28c), subject to (6a)-(6c), comprise three independent equations for ρ_2, p_2, and ξ_s (or v_s), thereby providing the necessary information to compute the flow variables in the whole domain $0 \le \xi < \infty$. Note that (28a)-(28c) can be written in the form

$$\frac{\mathrm{d}\ln v}{\mathrm{d}\ln \xi} = (\nu-1)\frac{c^2}{(\xi v_0 - v)^2 - c^2}, \tag{30a}$$

$$\frac{\mathrm{d}\ln \rho}{\mathrm{d}\ln \xi} = -(\nu-1)\frac{v(\xi v_0 - v)}{(\xi v_0 - v)^2 - c^2}, \tag{30b}$$

$$\frac{\mathrm{d}\ln p}{\mathrm{d}\ln \xi} = -(\nu-1)\frac{v(\xi v_0 - v)}{(\xi v_0 - v)^2 - c^2}\frac{\rho c^2}{p}, \tag{30c}$$

knowing the value of the variables p, ρ, and v at any position implies knowing the r.h.s. in (30a)-(30c) that corresponds to the rate of change for each of the variables. This is convenient when one needs to solve the problem backwards: determining the conditions at $\xi \to \infty$ that provides some particular properties at the shock, e.g., Chapman-Jouget condition $\mathcal{M}_2 = 1$. Properties in the the stagnant zone $0 < \xi < \xi_s$ are uniform and correspond to those right behind the shock ρ_2, p_2, and upstream flow conditions $\xi_s < \xi < \infty$ are those given by (30a)-(30c).

An example of the solution for reactive Noh problem is displayed in Fig. 6 for the spherical case $\nu = 3$ in a van der Waals gas with $\alpha_0 = a\rho_0^2/p_0 = 0.1$, $\beta_0 = b\rho_0 = 0.01$, and $\gamma = 7/5$. The far-field Mach number is fixed to $\mathcal{M}_0 = v_o/c_0 = 2.5$ and the dimensionless energy term $\mathcal{Q} = q\rho_{1s}/p_{1s}$ is varied. Since the upstream compression process is assumed isentropic and adiabatic, the factor $\mathcal{Q}$ does not affect the upstream profiles, but it does affect the shock position ξ_s. With respect to the non-reactive case $\mathcal{Q} = 0$, the endothermic case, computed with $\mathcal{Q} = -1$, renders a lower value of ξ_s (slower propagation speed) and higher values of pressure and density downstream. By way of contrast, the exothermic case, computed with the highest value of energy released given by the sonic flow downstream ($v_s = c_2$), which corresponds to $\mathcal{Q} = 16.3$ for the given upstream conditions, renders a higher value of ξ_s (higher propagation speed) and lower values of pressure and density downstream resulting from the expansion of hot products.

The expanding CJ-detonation resembles the classic Zel'dovich-Taylor (ZT) detonation[104,105], which describes the self-similar flow structure behind a constant-velocity CJ detonation originated at the center without an external initiating energy. As in the reactive Noh problem, the steadiness of the expanding wave makes the flow downstream homentropic. However, in the ZT detonation, the compressed gas zone can be split into two distinguished zones separated by a weak discontinuity: a stagnant gas flow for the inner region and a rarefaction-like profile for the region between the weak discontinuity and the detonation wave[106]. In our case, since there is an incoming flow converging ahead of the shock, a uniform, resting stagnant gas can be produced immediately behind the shock, as in the classic Noh solution. Our stability analysis is not applicable to ZT flows involving a centered rarefaction wave behind the CJ detonation front.

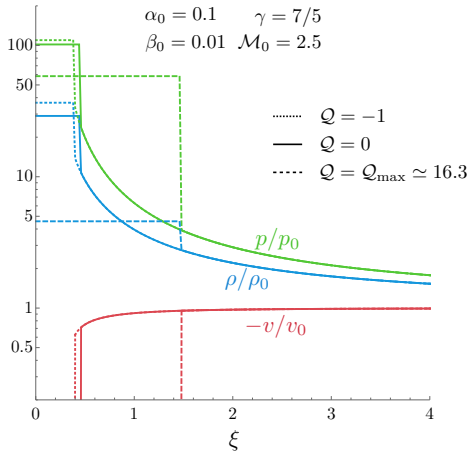

FIG. 6. Dimensionless pressure, density and velocity profiles for the spherical Noh problem ($\nu = 3$) in a van der Waals gas with $\alpha_0 = a\rho_0^2/p_0 = 0.1$, $\beta_0 = b\rho_0 = 0.01$ and $\gamma = 7/5$, with initial Mach number $\mathcal{M}_0 = 2.5$ and different values of $\mathcal{Q}$.

B. Linear perturbation analysis

The perturbation analysis presented next closely follows Ref.[59], where a detailed explanation is given. We then restrict the problem formulation and resolution to its minimum definitions, to focus on the effect of endothermcity and exothermicity. For a spherical geometry, the perturbed shock-front position $\delta r_s = r_s(\theta,\varphi,t) - v_s t$ is written in terms of spherical harmonics, i.e.,

$$\frac{\delta r_s}{v_s t} = \epsilon \sum_{l,m} \zeta_{l,m} \left(\frac{t}{t_0}\right)^{\sigma_{l,m}} Y_l^m(\theta,\varphi), \tag{31}$$

where v_s and $v_s t$ correspond to the unperturbed shock velocity and radial position of the shock, respectively, and $\theta \in [0,\pi]$ and $\varphi \in [0,2\pi]$ stand for the polar and azimuthal angles, respectively. The term proportional to the small-amplitude parameter $\epsilon \ll 1$ includes $Y_l^m(\theta,\varphi) = P_l^m(\cos\theta)\exp(\mathrm{i}m\varphi)$, where P_l^m is the associated (generalized) Legendre function with l and $m \leq l$ referring to the polar and azimuthal integer mode numbers. The complex amplitude of a given eigenmode is denoted by $\zeta_{l,m}$. The lack of scales dictates the power-law dependence $(t/t_0)^\sigma$, where t_0 is an arbitrary temporal parameter used to provide dimensional consistency and $\sigma_{l,m} = \sigma = \sigma_\mathrm{R} + \mathrm{i}\sigma_\mathrm{I}$ is the complex dimensionless eigenvalue. The stability condition then reduces to $\sigma_\mathrm{R} \leq 0$. A sketch of the spherical (a) and cylindrical (b) perturbed shocks is presented in Fig. 7.

Since all irreversible processes take place right behind the shock, within a zone of negligible thickness, the perturbations at the post-shock flow are governed by the linearized scale-free Euler equations, thereby imposing the perturbations $\delta\rho = \rho(\theta,\varphi,\eta,t) - \rho_2$, $\delta p = p(\theta,\varphi,\eta,t) - p_2$, $\delta v = v_r(\theta,\varphi,\eta,t)$ for the density, pressure and radial velocity disturbances. For convenience, the variable $\delta d = r\nabla_\perp \cdot \delta\boldsymbol{v}_\perp(\theta,\varphi,\eta,t)$ is introduced, which involves the components of the transverse velocity perturbations $\delta\boldsymbol{v}_\perp = \delta v_\theta \boldsymbol{e}_\theta + \delta v_\varphi \boldsymbol{e}_\varphi$. Separation of variables dictates

$$\bar{\rho} = \frac{\delta\rho}{\rho_2} = \epsilon \sum_{l,m} \left(\frac{t}{t_0}\right)^\sigma G(\eta) Y_l^m(\theta,\varphi), \tag{32a}$$

$$\bar{p} = \frac{\delta p}{\rho_2 c_2^2} = \epsilon \sum_{l,m} \left(\frac{t}{t_0}\right)^\sigma P(\eta) Y_l^m(\theta,\varphi), \tag{32b}$$

$$\bar{v}_r = \frac{\delta v}{c_2} = \epsilon \sum_{l,m} \left(\frac{t}{t_0}\right)^\sigma V(\eta) Y_l^m(\theta,\varphi), \tag{32c}$$

$$\bar{d} = \frac{\delta d}{c_2} = \epsilon \sum_{l,m} \left(\frac{t}{t_0}\right)^\sigma D(\eta) Y_l^m(\theta,\varphi), \tag{32d}$$

as the functional dependence of the perturbed flow variables, which are all proportional to $(t/t_0)^\sigma$ along any constant-speed trajectory, for example, at the shock position $r_s = v_s t$. This is because the corresponding eigenfunctions $G(\eta)$, $P(\eta)$, $V(\eta)$ and $D(\eta)$, are to be determined. They depend on the self-similar variable that is conveniently constructed with the speed of sound in the compressed gas

$$\eta = \frac{r}{c_2 t}, \tag{33}$$

which satisfies $\eta = \mathcal{M}_2 \xi/\xi_s$.

The main mode number $j \geq 0$ is used to unify the notation for both cylindrical and spherical geometries. The former is given by $\nu = 2$ and $j = m$ and the latter is represented by $\nu = 3$ and $j = l$. The substitution of the perturbed variables (32a)-(32d) into the Euler equations (23)-(25) yields a system of first-order differential equations that only involve geometrical parameters, ν and j:

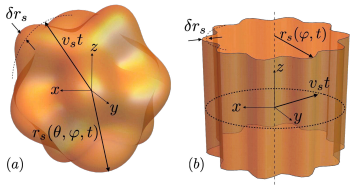

FIG. 7. Sketch of the spherical (a) and cylindrical (b) perturbed shocks. The perturbation amplitude is purposely magnified to facilitate its visualization.

$$\left(\sigma - \eta\frac{\mathrm{d}}{\mathrm{d}\eta}\right) G + \frac{\mathrm{d}V}{\mathrm{d}\eta} + \frac{(\nu-1)V}{\eta} + \frac{D}{\eta} = 0, \tag{34a}$$

$$\left(\sigma - \eta\frac{\mathrm{d}}{\mathrm{d}\eta}\right) V + \frac{\mathrm{d}P}{\mathrm{d}\eta} = 0, \tag{34b}$$

$$\left(\sigma - \eta\frac{\mathrm{d}}{\mathrm{d}\eta}\right) D - j(j+\nu-2)\frac{P}{\eta} = 0, \tag{34c}$$

$$\left(\sigma - \eta\frac{\mathrm{d}}{\mathrm{d}\eta}\right) (G - P) = 0. \tag{34d}$$

The integration of (34a)-(34d) to obtain $G(\eta)$, $V(\eta)$ $P(\eta)$ and $D(\eta)$ must be carried out with the aid of the boundary condition at the shock front, given by the four linearized conservation equations corresponding to the conservation of mass, radial momentum, tangential momentum and energy. After some straightforward algebra, they can be rewritten as

$$P_s = \frac{\mathcal{M}_2^2(\mathcal{R}-1)}{\mathcal{R}} \frac{2(\sigma+\nu) - \mathcal{R}(\nu-1)(1+h_1)}{1+h}, \tag{35a}$$

$$G_s = -\frac{\mathcal{R}-1}{\mathcal{R}} \frac{2h(\sigma+\nu) - \mathcal{R}(\nu-1)(h-h_1)}{1+h}, \tag{35b}$$

$$D_s = \mathcal{M}_2(\mathcal{R}-1)\, j(j+\nu-2), \tag{35c}$$

$$V_s = \frac{\mathcal{M}_2(\mathcal{R}-1)}{\mathcal{R}} \times \frac{(1-h)(\sigma+\nu) + \mathcal{R}(\nu-1)(h-h_1)}{1+h}, \tag{35d}$$

for the values of the sought eigenfunctions at $\eta = \mathcal{M}_2$.

The shock boundary condition assumes that the thickness of the non-equilibrium region is much smaller than the perturbation wavelength (thin shock limit), with the latter being much greater than the shock perturbation amplitude (linear theory).

The upstream flow is not uniform. A relatively advanced position of the shock will find lower density, lower pressure and higher velocity, as seen in Fig. 6. The opposite occurs for a local retarded position of the distorted shock. This affects the mass, radial and energy entrainment at the shock at a given shock location and

time. The influence of the upstream flow variations is accounted in the factor

$$h_1 = \frac{h}{\mathcal{M}_1^2 - 1}\left[\frac{1}{c_{s1}^2}\frac{\partial p_2}{\partial \rho_{1s}}\bigg|_{\rho_2, p_{1s}} + \frac{\partial p_2}{\partial p_{1s}}\bigg|_{\rho_2, \rho_{1s}}\right], \quad (36)$$

which takes the following form:

$$h_1 = \frac{\mathcal{M}_1^2}{\mathcal{R}^2\left(\mathcal{M}_1^2 - 1\right)}\left(\frac{\partial \mathcal{P}}{\partial \mathcal{R}}\right)^{-1}\left[\mathcal{R}\frac{\partial \mathcal{P}}{\partial \mathcal{R}} - \beta_1\frac{\partial \mathcal{P}}{\partial \beta_1} + (\gamma_{1s} - 2)\alpha_1\frac{\partial \mathcal{P}}{\partial \alpha_1} - \gamma_{1s}\mathcal{P} + \mathcal{Q}(\gamma_{1s} - 1)\frac{\partial \mathcal{P}}{\partial \mathcal{Q}}\right] (37)$$

for a reactive shock in a vdW gas. The partial derivatives of the pressure function $\mathcal{P}$ with respect to the dependent variables can be explicitly written with the aid of (10).

The Euler equations only involve geometrical parameters ν and j, but the Rankine-Hugoniot equations introduce four additional parameters: $\mathcal{R}$, $\mathcal{M}_2$, h and h_1. They are similar to those shown in Ref.[59], the difference relies on the values of the variables defining the shock properties for a given shock condition. For example, for an ideal gas, the four parameters can be expressed in terms of γ and $\mathcal{M}_1$, which means that two of them can be expressed, either explicitly or implicitly, as a function of the other two. For an ideal gas with a constant energy factor $\mathcal{Q}$, three parameters are needed to calculate $\mathcal{R}$, $\mathcal{M}_2$, h and h_1. For a vdW EoS, either adiabatic or not, all four of them are independent parameters.

The integration of (34a)-(34d) can be done analytically following the procedure detailed in Refs.[59,69] which can be summarized as follows. The pressure eigenfunction is only of acoustic type, while the density and velocity eigenfunctions are split into acoustic and entropic for the former and acoustic and vortical for the latter. The acoustic mode corresponds to reverberating waves whose amplitude in each fluid particle is time dependent. On the other hand, the entropic and vortical perturbations in each fluid particle are constant, their respective values being determined at the instant of this particle's passage through the shock front, after which its unperturbed radial position remains $r = v_s t$. In sum, the integration of (34a)-(34d) with the boundary condition at $\eta = \mathcal{M}_2$, can be used to compute the value of the three mode amplitudes and the eigenvalue σ, with the latter being determined by the dispersion relationship

$$\frac{\mathcal{R}(\nu - 1) - \sigma - \nu + \mathcal{R}j(j + \nu - 2)}{\sigma + \nu + j - 1}F_{1s}^{+} = \frac{\mathcal{R}(\nu - 1)\left(1 + h_1\right) - 2(\sigma + \nu)}{(1 + h)\left(\sigma + \nu - 1\right)}F_{1s}^{-}, \quad (38)$$

where the functions F_{1s}^{+} and F_{1s}^{-}, which refer to the Gauss hypergeometric functions evaluated at the shock front, can be defined conjointly as

$$F_{1s}^{\pm} = {}_2F_1\left(\frac{j - \sigma}{2}, \frac{j \pm 1 - \sigma}{2}; j + \frac{\nu}{2}; \eta^2 = \mathcal{M}_2^2\right). \quad (39)$$

IV. THE EIGENVALUES POOL

The eigenvalue σ that is solution of (38) can be computed numerically. For each combination of parameters ν and j, $\mathcal{R}$, $\mathcal{M}_2$, h and h_1 there exists an infinite number of complex conjugate eigenvalues satisfying (38). We define the radial mode number n that corresponds to the different eigenmodes, for a given value of j, in the order of increasing σ_{I}.

In order to study the effect of endothermicity and exothermicity in the unstable range $h > h_c$, as done for the planar isolated shock in Fig. 3, we choose the same gas properties as those employed by Refs.[3,59] associated with a highly compressible vdW gas with $\gamma = 31/30$, $\alpha_1 = 1/2$, and $\beta_1 = 1/9$. Thus, Fig. 8 displays the first seven (lowest frequencies) values of σ with three different values of the dimensionless energy factor corresponding to adiabatic $Q = 0$, endothermic $\mathcal{Q} = -1/2$ and exothermic cases $\mathcal{Q} = 1/2$. The perturbation mode numbers are $j = 10$, $j = 125$, $j = 200$, and $j = 350$, from left to right. Mode numbers are chosen to give four different results, presented as they progressively follow one another as the mode number increases: all are stable cases (a), only the endothermic case is unstable (b), only the exothermic case is stable (c), and all are unstable cases (d). It is observed that eigenvalues are all stable for low mode numbers, even if condition $h > h_c$ is satisfied. This is because of the stabilizing effect of the expanding domain. In contrast to what happens in planar shock geometry, in cylindrical or spherical configurations the expansion of the front attenuates the amplitude of the acoustic waves reaching the shock from behind. As j increases the expansion effect weakens and the set of complex eigenvalues moves to the positive half-plane $\sigma_{\mathrm{R}} > 0$, being that associated with the lowest oscillation frequency the one that crosses first the axis $\sigma_{\mathrm{R}} = 0$, thereby setting the stability threshold. If we were analyzing a case with $h < h_c$, the crossing to the positive half space will never occur, i.e., $h > h_c$ is a necessary, but not sufficient, condition for shock instability because the mode number j must be sufficiently large. Similar computations in spherical geometry shows a qualitatively similar picture, but the required mode numbers to get the four different cases are higher as the stabilizing effect of shock divergence is more pronounced for $\nu = 3$.

In what concerns the effect of endothermicity/exothermicity, it is found that endothermic shocks $\mathcal{Q} < 0$ are the first to become unstable with the same EoS properties and shock compression ratio. Then follows the adiabatic $\mathcal{Q} = 0$ and the exothermic $\mathcal{Q} > 0$ cases, in agreement with Fig. 3 for planar shocks. By increasing the mode number we can find multiple poles in the region $\sigma_{\mathrm{R}} > 0$, although the first to cross is the one with the largest σ_{R} and therefore, the dominant one.

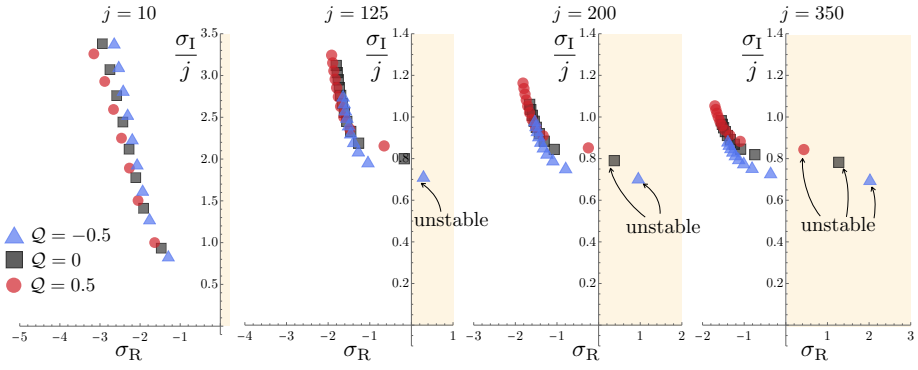

FIG. 8. Eigenvalues for an expanding cylindrical shock ($\nu = 2$) with $\mathcal{R} = 2.9$ in a vdW gas EoS with $\gamma = 31/30$, with $\alpha_1 = 1/2$, and $\beta_1 = 1/9$ and different energy values $\mathcal{Q} = -0.5$, 0 and 0.5. Four mode numbers are chosen: $j = 10$, $j = 125$, $j = 200$, and $j = 350$.

A. Radial acoustic modes

Radial modes correspond to those where acoustic waves reverberate normally to the shock front. Then, this limit resembles the case of a one-dimensional shock front that is perturbed in velocity with no associated corrugation. The acoustic wave number then points in the shock propagation direction. In our case, it corresponds to the case $n \gg j$ given by the short-wavelength limit $\sigma_I \to \infty$, with σ_R and j finite.

The multiple-frequency character of the solution stems from the closed domain between the shock and the center (or axis of symmetry). Then, an isolated shock only exhibits a fundamental oscillation frequency, as discussed below. As detailed in Refs.[59,69], the relation between subsequent frequencies reads as

$$\sigma_I^{(n\gg j)} \sim \frac{2\pi n}{\ln \mathscr{D}_s} + O(1), \tag{40}$$

which accounts for the expanding domain effect through the Doppler shift factor

$$\mathscr{D}_s = \frac{1+\mathcal{M}_2}{1-\mathcal{M}_2} > 1. \tag{41}$$

The real part of the eigenvalue that characterizes the decay/growth rate depends, not only on the Doppler shift factor, but also on the reflection coefficient $\mathscr{R}_s$ in the following form:

$$\sigma_R^{(n\gg j)} \sim -\frac{\nu-1}{2} + \frac{\ln|\mathscr{R}_s|}{\ln \mathscr{D}_s}, \tag{42}$$

where

$$\mathscr{R}_s = \frac{2\mathcal{M}_2 - 1 + h}{2\mathcal{M}_2 + 1 - h} \tag{43}$$

measures the amplitude change of an acoustic wave that impinges on the shock from behind.

The real part of the eigenvalues in the radial limit, given by (42), yields $\sigma_R(n \gg j) = -2.66$, -2.63, and -2.61 for the conditions displayed in Fig. 8 that correspond to $\mathcal{Q} = -0.5$, $\mathcal{Q} = 0$ and $\mathcal{Q} = 0.5$, respectively. Then, the eigenvalues for $n \gg j$ are all stable and, moreover, they are not the ones with a lower decay rate. This is not necessarily true for all EoS. For example, a similar perturbation analysis for an inert shock in an ideal gas EoS with $\gamma = 7/5$ shows that the $\sigma_R(n \gg j)$, although negative, gives the less negative of the complex eigenvalues pool, then being the dominant ones in describing the shock dynamics.

From the reflection coefficient, we find that $\mathscr{R}_s > 1$ if $1 < h < 1 + 2\mathcal{M}_2$, so acoustic waves are amplified upon reflection from the shock front. When considering a planar shock with no corrugation, just a perturbation in the propagation speed, this condition indicates shock instability, in agreement with Refs.[88,93]. However, the geometry plays a role in the stability limits. By doing $\sigma_R(n \gg j) = 0$ in (42), we find that the unstable range for all cases ($\nu = 1$, 2, and 3) is

$$1 + 2\mathcal{M}_2 \frac{\mathscr{D}_s^{\frac{\nu-1}{2}} - 1}{\mathscr{D}_s^{\frac{\nu-1}{2}} + 1} < h < 1 + 2\mathcal{M}_2, \tag{44}$$

with the lower boundary corresponding to $\sigma_R(n \gg j) = 0$. It indicates that the condition for instability is harder to meet in expanding shocks because the factor accompanying 1 in the lower boundary is greater than unity for $\nu > 1$. The upper boundary does not change with geometry as it corresponds to an unstable condition for the Rankine-Hugoniot equation irrespective of the supporting condition. We find that as h increases from the lower to the upper boundary of the range (44), the cor-

responding power index $\sigma_{\rm R}(n \gg j)$ increases from zero to infinity.

It is readily seen that the Doppler factor (41) diverges in the CJ limit because acoustic waves downstream move at the same speed as the shock front, thereby impeding them to catch up the shock from behind. On the other hand, the reflection coefficient (43) drops to zero, as $h \to -1$ in this limit. Interestingly however, the two coefficients share the same leading order contribution, thereby making the asymptotic function (42) converge to $\sigma_{\rm R} \to -(\nu+1)/2$ in the CJ limit. On the other hand, the factor $2\pi n/\ln \mathscr{D}_s$ in (40) goes to zero for $\mathcal{M}_2 \to 1$, so the infinite set of complex poles tends to occupy the same position in the complex plane of Fig. 8. Another interesting feature of the CJ limit is observed in (44), since the instability region collapses to a single value of the DK parameter, namely $h = 3$.

The approach to the singular conditions of the CJ limit is better described with the aid of Fig. 9(a) and (c), that shows the asymptotic expressions of the eigenvalues in the radial limit as a function of $\mathcal{Q}_{\max} - \mathcal{Q}$ for different mass compression ratios $\mathcal{R}$. For simplicity, and because it does not affect the analysis, it is chosen an ideal gas EoS ($\alpha_1 = 0$, $\beta_1 = 0$) with $\gamma = 5/3$. As the factor $\mathcal{Q}_{\max} - \mathcal{Q}$ decreases (or $\mathcal{M}_2 \to 1$), the reactive shock becomes more self-supported. Figure 9(a) shows that $\sigma_{\rm R} \to -(\nu+1)/2 = -3/2$ when $\mathcal{Q}$ approaches its maximum value. On the other side, $\sigma_{\rm R} \to -(\nu+1)/2 - 2 = -7/2$ in the adiabatic limit $\mathcal{Q} \to 0$. This is a singular result obtained only for $\gamma = 5/3$, as asymptotically derived in Ref.[69]. Other values of γ render a shock-strength dependent value of the eigenvalue in the radial limit[69]. It is also found that, as $\mathcal{R} \to \mathcal{R}_{\rm cj,max}$, the curve becomes stiffer because $\mathcal{R} = \mathcal{R}_{\rm cj,max}$ implies $\mathcal{Q} = \mathcal{Q}_{\max}$ by definition. Therefore, when $\mathcal{R} = \mathcal{R}_{\rm cj,max}$ it is either at CJ conditions for $\mathcal{Q} > 0$ or it is a regular adiabatic shock for $\mathcal{Q} = 0$. In any case, CJ conditions predict oscillation with lower decay rate for the radial modes. Figure 9(c) shows the frequency variation between correlative eigenmodes as a function of $\mathcal{Q}_{\max} - \mathcal{Q}$. As anticipated, this value tends to zero because $\mathcal{M}_2 \to 1$ in this limit. However, because of the logarithm dependence, this decay is remarkably slow.

Let's now explore the opposite case corresponding to endothermic shocks. The same asymptotic magnitudes are computed now in Fig. 9(b) and (d) as a function of $\mathcal{Q} - \mathcal{Q}_{\min}$, where $\mathcal{Q}_{\min} < 0$, for different values of the mass compression ratio $\mathcal{R}$. In this case, as the factor $\mathcal{Q} - \mathcal{Q}_{\min}$ decreases, the shock wave propagation speed, relative to the upstream gas, approaches the sonic condition $\mathcal{M}_1 \to 1$. This limit renders finite and non-singular values for $\mathcal{M}_2$ and h, which are the parameters that ultimately describe the shock stability in the radial limit. Therefore, this case is not particularly distinctive to any other condition associated with an adiabatic shock, beyond the quantitative differences. In agreement with panel (a), Fig. 9(b) shows that $\sigma_{\rm R} \to -(\nu+1)/2 - 2 = -7/2$ in the adiabatic limit $\mathcal{Q} \to 0$. However, for finite values

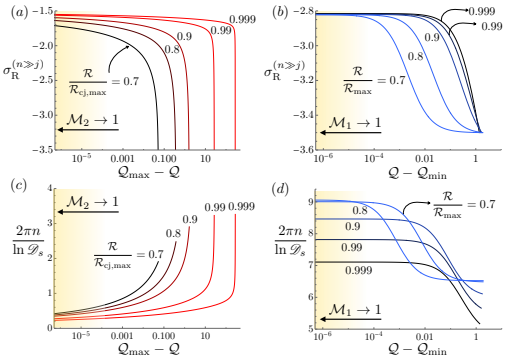

FIG. 9. Asymptotic expressions of the eigenvalues in the radial limit as a function of the displaced energy factor $\mathcal{Q}$ for different values of the mass compression ratio $\mathcal{R}$. Panels (a) and (b) show $\sigma_{\rm R}$ in exothermic and endothermic cases, respectively, and panels (c) and (d) display frequency variation between correlative eigenmodes in exothermic and endothermic cases, respectively. Results are computed for a cylindrical shock ($\nu = 2$) in an ideal gas ($\alpha_1 = 0$, $\beta_1 = 0$) with $\gamma = 5/3$.

of $\mathcal{Q} < 0$, the effect of increasing the mass compression ratio $\mathcal{R}$ is the opposite to that found in exothermic shocks. With regard to the frequency of the oscillations, increasing the energy subtracted amplifies the variation between correlative eigenmodes because the post-shock Mach number decreases with the endothermicity degree.

B. Transverse acoustic modes

Relation (44) gives sufficient rather than necessary instability conditions, since instability may occur even if $\sigma_{\rm R}(n \gg j) < 0$. This is readily seen in Fig. 8, where increasing the mode number j may lead to instability and this occurs for the eigenvalue with the lowest frequency $n = 1$. It is then convenient to evaluate the opposite limit, $j \gg n$, associated with short perturbation wavelengths. In this case, the shock-ripple oscillation frequency corresponds to the fundamental frequency occurring in planar shocks

$$\frac{\sigma_{\rm I}^{(j\gg n)}}{j} \to \frac{\sqrt{1-\mathcal{M}_2^2}}{\mathcal{M}_2}. \tag{45}$$

This can be easily deduced with the aid of Fig. 10 that sketches the time that needs an acoustic wave to cover a wavelength distance in the transverse direction. Since the sonic wave moves at velocity c_2 and the shock moves with velocity $v_s = u_2 < c_2$, the distance needed to travel a λ unit along the transverse direction is $c_2\Delta t$, while the shock moves frontwards a distance $v_s\Delta t$. We have $\lambda^2 = (\Delta t)^2(c_2^2 - v_s^2)$ by construction, that finally renders

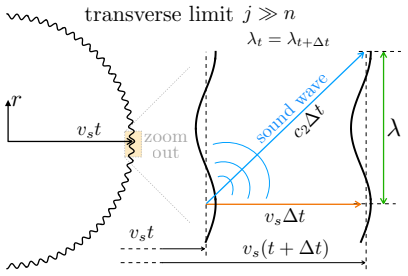

FIG. 10. Sketch of the acoustic interaction along the shock surface in the short wavelength limit.

$\lambda/(v_s\Delta t) = \sqrt{1-\mathcal{M}_2^2}/\mathcal{M}_2$ as the dimensionless characteristic frequency, in agreement with (45). Note that different normalization yields $\lambda/(c_2\Delta t) = \sqrt{1-\mathcal{M}_2^2}$.

Evaluating $\sigma_{\rm I}(j \gg n)/j$ for the conditions computed in Fig. 8(d) we obtain 0.68, 0.76, and 0.82 for $\mathcal{Q} = -0.5$, $\mathcal{Q} = 0$ and $\mathcal{Q} = 0.5$, respectively, which fairly correspond to the scaled frequency of the leading eigenvalues, those in the half-plane $\sigma_{\rm R} > 0$. They are order-of-unity values of the relative oscillation frequency. However, if we evaluate the CJ limit $\mathcal{M}_2 \to 1$ the relative oscillation frequency drops to zero, i.e., there is no actual oscillation. It stems from the fact that the effective acoustic time that needs an acoustic wave to cover a wavelength in the transverse direction, Δt, tends to infinity, as sketched in Fig. 10, when $v_s \to c_2$. Therefore, in the CJ limit, different positions of the shock front get acoustically decoupled. In such case, the inner structure of the detonation front cannot be neglected, since the local Mach number is lower than unity within the reaction zone. The inclusion of the reaction region adds a characteristic scale in the perturbation analysis, and that impedes the use of the proposed separation of variables with the self-similar coordinate. Moreover, CJ detonations are known to be strongly unstable as it involves an exponential thermal sensitivity, exhibiting in many cases the so-called cellular instability[73,86].

Although the limit $j \gg n$ recovers the characteristic oscillation frequency of a planar shock, the expanding-shock configuration should be evaluated with finite mode numbers. In such case, the divergence effect is always noticeable. To evaluate the transition towards the limit $j \to \infty$, the value $\sigma_{\rm I}^n/j$ is computed in Fig. 11 for different conditions of exothermicity/endothermicity. Among the multiple solutions corresponding to all solutions of the dispersion equation, Fig. 11 shows the one that dominates for $j \gg 1$, which typically corresponds to $n = 1$. Computations are all carried out for a cylindrical shock ($\nu = 2$) with $\mathcal{R} = 1.5$. Different EoS are studied: an ideal monatomic gas (a) and a vdW gas (b), corresponding to decaying and non-decaying (SAE) for an isolated non-reactive planar case, respectively. It is observed that,

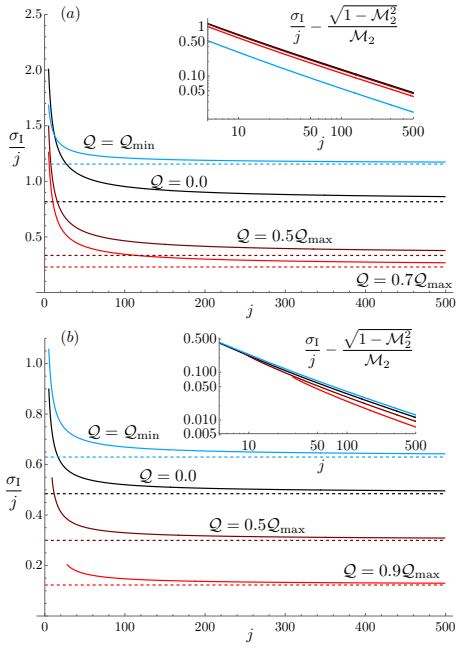

FIG. 11. Asymptotic expressions of the imaginary part of the eigenvalues that satisfy $\sigma_{\rm R} = 0$ compared to the asymptotic limit $j \gg n$ as a function of the mode number j. Computations are all done for a cylindrical shock ($\nu = 2$) with a finite mass compression ratio $\mathcal{R} = 1.5$. Panel (a) corresponds to an ideal monatomic gas ($\alpha_1 = 0$, $\beta_1 = 0$, $\gamma = 5/3$) and (b) to a vdW gas ($\alpha_1 = 1/2$, $\beta_1 = 1/9$, $\gamma = 31/30$) .

regardless the conditions, stable or unstable, $\sigma_{\rm I}/j$ approaches the asymptotic value $\sqrt{M_2^{-2}-1}$ when $j \to \infty$, as previously anticipated. The inset shows that the approach towards the transverse limit requires very large values of j, of the order of 10^3 to obtain the 99% of the asymptotic value. This evidences that the effect of divergence will be noticeable in most practical applications. Considering a spherical shock wave does not change the qualitative results, but will demand higher values of j to effectively approach to the planar limit. We recall that $\sigma_{\rm I}/j$ approaches 0 when $\mathcal{Q} \to \mathcal{Q}_{\rm max}$ (or $\mathcal{M}_2 \to 1$) and that endothermic shocks oscillate with higher frequency because $\mathcal{M}_2$ is lower.

V. THE STABILITY LIMITS

In Sec.IV, we have numerically evaluated the poles of the dispersion relationship (38) in conditions where a planar non-reactive isolated shock renders SAE, see Sec.II.

We found that $\mathcal{Q} < 0$ promotes instability in the sense that the difference $h - h_c$ increases as well as the domain where the DK condition is satisfied. Unlike in the planar shock case, the value of h has an impact in the growth rate for $h > h_c$ in steady expanding shocks, and so will have the value of $\mathcal{Q}$. For example, we have analyzed the effect of endothermicity and exothermicity on the theoretical limits corresponding to dominantly radial $n \gg j$ and transverse perturbations $j \gg n$, previously derived in Refs.[59,69]. We found that the case $n \gg j$ is more restrictive to yield instability because the mechanism of unstable growth relies on having a reflection coefficient greater than unity. The condition for instability in the transverse limit $j \gg n$ will be discussed below.

Let's first evaluate the stability of steady expanding shocks for finite mode numbers j. As illustrated in Fig. 8, the real part of the eigenvalue could be positive or negative depending on the specific conditions, thereby rendering unstable or stable conditions, respectively. The interest is placed in the identification of the stability threshold that corresponds to a purely imaginary eigenvalue, $\sigma_{\rm R} = 0$. To determine its location, we solve (38) for h and substitute an imaginary value of $\sigma = is$, where s is real and positive, into the result, arriving at

$$\hat{h}(s) = -1 - \left.\frac{F_{1s}^{-}}{F_{1s}^{+}}\right|_{\sigma=is} \times \frac{\Big[2(is+\nu) - \mathcal{R}(\nu-1)\,(1+h_1)\Big](is+\nu+j-1)}{(is+\nu-1)\Big[\mathcal{R}(\nu-1) - is - \nu\Big] + \mathcal{R}\,j(j+\nu-2)}. \tag{46}$$

For an arbitrary value of s, the right-hand side of (46) is complex, implying that $\sigma = is$ is not a physically meaningful eigenvalue because h must be real, so that $\mathrm{Im}[\hat{h}(s)] = 0$. This equation provides an infinite number of solutions that are actual eigenvalues and that correspond to conditions where complex eigenvalues cross the line $\sigma_{\rm R} = 0$, each of them being associated with a different value of h. The lowest of these values is the instability threshold for the DK parameter, denoted by $h_{st}(\mathcal{M}_2, \mathcal{R}, h_1, \nu, j)$. Notice that there exists an infinite number of solutions corresponding to different oscillation frequencies $\sigma = 0 \pm i\sigma_1^{(n)}$, where n is the radial number defined previously.

To evaluate the effect of $\mathcal{Q}$ in the stability limits, we show the iso-curves $\sigma_{\rm R} = 0$ on the plane $\mathcal{R} - j$, for different conditions of endothermicity/exothermicity. This is illustrated in Fig. 12, which has been computed with EoS properties that render SAE in planar geometry ($h > h_c$) in a finite interval of mass compression ratio, as in Fig. 3. Then, the factor $\mathcal{Q}$ is varied to investigate its effect. The stabilizing effect of the expanding shock is readily seen: there exists a minimum value of $j = j_{\rm min}$, below which the shock is stable for any shock compression ratio $\mathcal{R}$. For cylindrical and spherical geometries in non-reactive gases, we find $j_{\rm min} = 148$ and 213, respectively, which occur at $\mathcal{R} \sim 2.8$. However, modifying the degree of endothermicity/exothermicity changes the instability

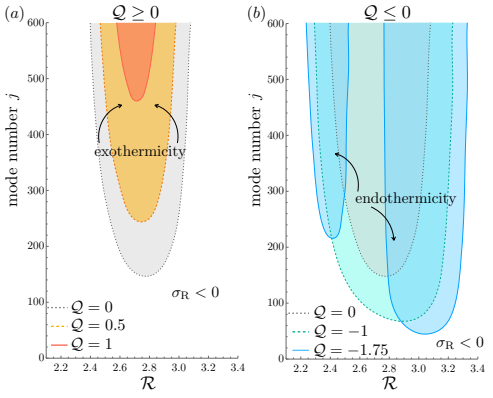

FIG. 12. Unstable regions as a function of the mass compression ratio $\mathcal{R}$ and the mode number j for different values of the energy factor $\mathcal{Q}$, exothermic cases in panel (a) and endothermic in panel (b). Results are computed for a cylindrical shock ($\nu = 2$) in a vdW gas ($\alpha_1 = 1/2$, $\beta_1 = 1/9$) with $\gamma = 31/30$.

boundary, as the values of h and h_{st} implicitly depend on $\mathcal{Q}$, in a similar fashion to that computed in Fig. 4 for planar shocks. Qualitatively, the higher is the difference $h - h_c > 0$, the higher will be $h - h_{st} > 0$. For example, the higher is the heat release the more stable is the expanding shock. If $\mathcal{Q}$ is sufficiently large so that $h < h_c$, the shock will be stable regardless the mode number. On the other hand, endothermicity exhibits an opposite effect: the minimum mode number to render instability decreases, yet the unstable region splits into two different regions, as anticipated in Fig. 3 that would correspond to the instability boundaries for $j \to \infty$. Note that a spherical shock, $\nu = 3$, displays a similar pattern with the unstable regions will being roughly shifted upwards, i.e., the condition for instability calls for higher mode numbers.

The asymptotic limits $j \gg n$, to which the limits of the unstable regions tend, correspond to the zeros of the function $h - h_c$ displayed in Fig. 3. This is equivalent as saying that

$$h_{st}(\mathcal{M}_2, \mathcal{R}, h_1, \nu, j) \to h_c(\mathcal{M}_2, \mathcal{R}) \tag{47}$$

when $j \to \infty$, for any set of shock conditions (exothermicity/endothermicity) and geometrical properties (spherical/cylindrical).

For finite values of j, we find $h_{st} > h_c$, so that the condition for instability is harder to meet. However, (47) does not provide information of the next leading-order contribution which could be used to theoretically analyze the contribution of j for large values of the mode number. We have not found in the literature the expansion of Gauss hypergeometric functions (or the equivalent Legendre associated functions) with complex arguments

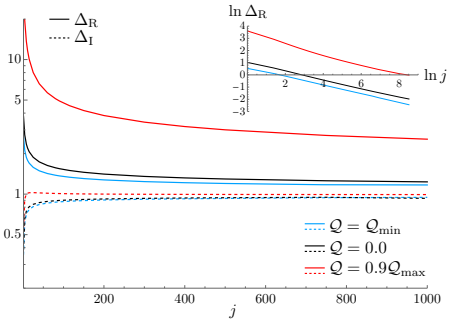

FIG. 13. Functions Δ_R and Δ_R that satisfy as a function of the mode number j. Computations are all done for a cylindrical shock ($\nu = 2$) with and $\mathcal{R} = 1.5$ in a vdW gas with $\alpha_1 = 1/2$, $\beta_1 = 1/9$ and $\gamma = 31/30$.

in the limit $j \gg n$. The only available relation is the asymptotic short-wavelength limit

$$\lim_{j\to\infty} \frac{F_{1s}^-}{F_{1s}^+}\bigg|_{\sigma=ij\sqrt{\mathcal{M}_2^{-2}-1}} = 1 - \mathcal{M}_2^2 + i\mathcal{M}_2\sqrt{1-M_2^2} \quad (48)$$

that does not depend on ν for $j \to \infty$. Then, a direct numerical analysis is performed to demonstrate the validity of (47). In particular, the following parameters:

$$\Delta_R = \frac{1}{1-\mathcal{M}_2^2}\mathrm{Re}\left(\frac{F_{1s}^-}{F_{1s}^+}\bigg|_{\sigma=ij\sqrt{\mathcal{M}_2^{-2}-1}}\right), \quad (49)$$

$$\Delta_I = \frac{1}{\mathcal{M}_2\sqrt{1-\mathcal{M}_2^2}}\mathrm{Im}\left(\frac{F_{1s}^-}{F_{1s}^+}\bigg|_{\sigma=ij\sqrt{\mathcal{M}_2^{-2}-1}}\right), \quad (50)$$

are introduced to evaluate the transverse limit, since Δ_R and Δ_I approach unity for $j \to \infty$. These parameters are computed in Fig. 13 as a function of the mode number up to $j = 1000$. It is observed that, regardless the degree of endothermicity and exothermicity, both real and imaginary parts of F_{1s}^-/F_{1s}^+ for $\sigma = ij\sqrt{\mathcal{M}_2^{-2}-1}$ approach their asymptotic short-wavelength values, $1-\mathcal{M}_2^2$ and $\mathcal{M}_2\sqrt{1-M_2^2}$, respectively. The case close to the CJ limit, however, exhibits a much lower approach in what concerns the function Δ_R, which can be seen to come nearer unity in the inset. This is because the approach to the sonic condition downstream is associated with a longer characteristic time, as discussed in Fig.10. Per the imaginary part Δ_I, the approach towards unity is not monotonic, yet the function ultimately gets a clearer trend towards its asymptotic prediction.

VI. CONCLUSIONS

The stability of expanding shock waves that induce endothermic and exothermic effects has been addressed. For this purpose, use has been made of the so-called generalized Noh problem, extended to non-adiabatic shocks, to compute the perturbation-free solution. Although the problem can be formulated for an arbitrary EoS, a vdW gas has been employed because it has been proved to give non-decaying acoustic emission in the conditions found by J.W. Bates and D.C. Montgomery[3] for planar isolated shocks.

The results presented here indicate that endothermic and exothermic effects, here assumed to be independent of the post-shock properties, act markedly on the stability in a number of important ways with respect to the results predicted by adiabatic shocks. A breakdown of the results is offered:

(a) For planar isolated shocks, in conditions where the adiabatic isolated planar shock renders SAE, the effect of endothermicity is to widen the unstable range in the shock-compression ratio domain, with the possibility of splitting the unstable range into two separated zones. On the other hand, exothermicity has an opposite effect and sufficiently exothermic shocks may give rise to acoustically stable shocks for any shock strength.

(b) The generalized Noh problem admits self-similarity for shocks that induce endothermic or exothermic effects across the shock so long the shock plus the reaction zone can be treated as a single discontinuity. The restrictions on the energy substracted or delivered across the shock are imposed by the sonic conditions upstream and downstream, respectively.

(c) In agreement with adiabatic shocks, the DK instability of expanding steady shock waves drives a power-law growth of shock ripples and other flow perturbations in the range $h_c < h < 1 + 2\mathcal{M}_2$ deemed marginally stable in the classic theory[1,2,85]. The difference between this case and the classic case of isolated planar shock is due to the piston supporting the steady shock and represented with the center or axis of symmetry.

(d) The case associated with dominant radial modes, $n \gg j$, is more restrictive to yield instability because the mechanism of unstable growth relies on having a reflection coefficient greater than unity. The instability threshold in the transverse limit $j \gg n$ is the same as that for planar shocks $h > h_c$. Therefore, being in the unstable region for a planar shock is a sufficient, but not a necessary condition for the steady expanding shock to be unstable for finite mode numbers j.

(e) Divergence of the flow in cylindrical and spherical shocks has a stabilizing effect, but the center/axis of symmetry, which play the role of the piston in a planar shock, changes the character of the instability. The role of endothermicity and exothermicity is qualitatively similar to that found in planar

shocks, see item (a). For exothermic shocks close to the CJ condition (sonic flow downstream), the acoustic coupling becomes ineffective and the shock oscillation frequency drops to zero.

(f) The modification of the stability limits by endothermic/exothermic effects in a DK unstable vdW gas (with the EoS properties prescribed in Ref.[3]) is found to occur at relatively low values of the dimensionless energy factor $\mathcal{Q}$, thereby being associated with low concentration of the active species responsible of the non adiabaticity within the shock structure.

A more realistic model should include a variable energy factor in endothermic shocks, with the corresponding description of the phenomenon responsible of the energy variation (as done for example in planar dissociating shocks[8,11]). For exothermic shocks, the inclusion of the inner structure that may develop its own unstable evolution[73], would complete the global stability picture for non-adiabatic shocks. Nonetheless, the presence of the characteristic chemical time would impede the use of separation of variables and the analysis should be done with a different approach to that employed here. For similar reasons, the extension to include axial perturbations in cylindrical expanding shocks should be formulated with a different technique. Regardless the case, the findings reported in this work would greatly benefit from comparisons with numerical simulations in future works.

ACKNOWLEDGMENTS

A.C.R and C.H. work has been supported with project PID2019-108592RB-C41 (MICINN/FEDER, UE). C.H. work has been also supported by the Madrid Government (Comunidad de Madrid-Spain) under the Multiannual Agreement with UC3M (H2SFE-CM-UC3M). A.L.V. work has been supported by the National Nuclear Security Administration of the U.S. Department of Energy.)

DATA AVAILABLITY

The data that support the findings of this study are available from the corresponding author upon reasonable request.

REFERENCES

[1]S. D'yakov, Zh. Eksp. Teor. Fiz **27**, 288 (1954).
[2]V. Kontorovich, Zh. Eksp. Teor. Fiz **33**, 1525 (1957).
[3]J. W. Bates and D. C. Montgomery, Physical Review Letters **84**, 1180 (2000).
[4]I. V. Lomonosov, V. E. Fortov, K. V. Khishchenko, and P. R. Levashov, in *AIP Conference Proceedings* (vol 505, p.85–58, AIP, 2000).
[5]A. V. Konyukhov, A. P. Likhachev, V. E. Fortov, K. V. Khishchenko, S. I. Anisimov, A. M. Oparin, and I. V. Lomonosov, JETP Letters **90**, 18 (2009).
[6]A. Konyukhov, P. Levashov, and A. Likhachev, J. Phys. Conf. Ser. **1556**, 012022 (2020).
[7]A. Kulikovskii, A. Il'ichev, A. Chugainova, and V. Shargatov, J. Exp. Theor. Phys. **131**, 481 (2020).
[8]M. Mond and I. Rutkevich, Journal of Fluid Mechanics **275**, 121 (1994).
[9]M. Mond, I. M. Rutkevich, and E. Toffin, Physical Review E **56**, 5968 (1997).
[10]N. Wetta, J.-C. Pain, and O. Heuzé, Physical Review E **98**, 033205 (2018).
[11]C. Huete, F. Cobos-Campos, E. Abdikamalov, and S. Bouquet, Physical Review Fluids **5**, 113403 (2020).
[12]C. Huete and M. Vera, Journal of Fluid Mechanics **879**, 54 (2019).
[13]G. Duvall and R. Graham, Reviews of Modern Physics **49**, 523 (1977).
[14]R. Van Dongen, *Shock Wave Science and Technology Reference Library, Vol. 1: Multiphase Flows I*, Vol. 1 (Springer Science & Business Media, 2007).
[15]R. Griffiths, R. Sandeman, and H. Hornung, Journal of Physics D: Applied Physics **9**, 1681 (1976).
[16]A. Houwing, R. Sandeman, and G. Fowles, Shock Tubes and Waves , 277 (1984).
[17]O. Heuze, J.-C. Pain, and G. Salin, in *AIP Conference Proceedings*, Vol. 1195 (American Institute of Physics, 2009) pp. 103–106.
[18]M. Das, C. Bhattacharya, and S. V. G. Menon, Journal of Applied Physics **110**, 083512 (2011).
[19]C. Michaut, C. Stehlé, S. Leygnac, T. Lanz, and L. Boireau, The European Physical Journal D-Atomic, Molecular, Optical and Plasma Physics **28**, 381 (2004).
[20]I. Lomonosov and N. Tahir, Applied Physics Letters **92**, 101905 (2008).
[21]W. J. M. Rankine, Phil. Trans. Roy. Soc. London **160**, 277 (18818709).
[22]H. Hugoniot, J. Ec. Polyt. Paris **57**, 3 (1887).
[23]H. Hugoniot, J. Ec. Polyt. Paris **55**, 1 (1889).
[24]J. Johnson, *The SESAME database*, Tech. Rep. (Los Alamos National Lab.(LANL), Los Alamos, NM (United States), 1994).
[25]H. A. Bethe, in *Classic papers in shock compression science* (Springer, 1998) pp. 421–495.
[26]Y. B. Zel'dovich and Y. P. Raizer, *Physics of shock waves and high-temperature hydrodynamic phenomena* (Courier Corporation, 2002).
[27]V. Fortov, L. Al'tshuler, R. Trunin, and A. Funtikov, Shock waves and extreme states of matter (2004).
[28]S. Eliezer, *Fundamentals of equations of state* (Allied Publishers, 2005).
[29]R. Span, *Multiparameter equations of state: an accurate source of thermodynamic property data* (Springer Science & Business Media, 2013).
[30]V. Fortov, *Intense Shock Waves on Earth and in Space* (Springer International Publishing, 2021).
[31]R. F. Trunin, Physics-Uspekhi **37**, 1123 (1994).
[32]A. Kritcher, T. Döppner, D. Swift, J. Hawreliak, G. Collins, J. Nilsen, B. Bachmann, E. Dewald, D. Strozzi, S. Felker, *et al.*, High Energy Density Physics **10**, 27 (2014).

[33]D. C. Swift, A. L. Kritcher, J. A. Hawreliak, A. Lazicki, A. MacPhee, B. Bachmann, T. Döppner, J. Nilsen, G. W. Collins, S. Glenzer, *et al.*, Review of Scientific Instruments **89**, 053505 (2018).
[34]J. Nilsen, A. L. Kritcher, M. E. Martin, R. E. Tipton, H. D. Whitley, D. C. Swift, T. Döppner, B. L. Bachmann, A. E. Lazicki, N. B. Kostinski, *et al.*, Matter and Radiation at Extremes **5**, 018401 (2020).
[35]A. A. Avramenko, I. V. Shevchuk, and N. P. Dmitrenko, Journal of Non-Equilibrium Thermodynamics **in print** (2022).
[36]P. Gupta, R. K. Chaturvedi, and L. Singh, Waves in Random and Complex Media , 1 (2022).
[37]N. Zhao, A. Mentrelli, T. Ruggeri, and M. Sugiyama, Physics of fluids **23**, 086101 (2011).
[38]G. De Nittis and A. Moro, Proceedings of the Royal Society A: Mathematical, Physical and Engineering Sciences **468**, 701 (2012).
[39]J. D. Van Der Waals, *On the continuity of the gaseous and liquid states* (edited by J. S. Rowlinson (Courier Corporation), 2004).
[40]L. Landau and K. Stanyukovich, *Unsteady motion of continuous media* (Academic Press, New York, 1960).
[41]A. Medvedev, in *High-Pressure Shock Compression of Solids VII* (Springer, 2004) pp. 403–435.
[42]J. J. Martin and Y.-C. Hou, AIChE Journal **1**, 142 (1955).
[43]G. Guderley, Luftfahrtforschung **19**, 302–312 (1942).
[44]G. I. Taylor, Proceedings of the Royal Society of London. Series A. Mathematical and Physical Sciences **201**, 159 (1950).
[45]S. Anisimov and V. Kravchenko, Zeitschrift für Naturforschung A **40**, 8 (1985).
[46]L. I. Sedov, *Similarity and dimensional methods in mechanics* (CRC press, Boca Raton, USA., 1993).
[47]G. M. Bam-Zelikovich, Collection of Papers, no. 4 (ed. L. I. Sedov) **4** (1949).
[48]R. A. Axford, Laser and Particle Beams **18**, 93 (2000).
[49]L. V. Ovsiannikov, *Group analysis of differential equations* (Academic Press, 1982).
[50]C. Wu and P. Roberts, Quarterly Journal of Mechanics and Applied Mathematics **49**, 501 (1996).
[51]P. Roberts and C. Wu, Physics Letters A **213**, 59 (1996).
[52]S. Ramsey, Z. Boyd, and S. Burnett, Shock Waves **27**, 477 (2017).
[53]S. D. Ramsey, E. M. Schmidt, Z. M. Boyd, J. F. Lilieholm, and R. S. Baty, Physics of Fluids **30**, 046101 (2018).
[54]S. C. Burnett, K. G. Honnell, S. D. Ramsey, and R. L. Singleton, Journal of Verification, Validation and Uncertainty Quantification **3** (2018).
[55]S. D. Ramsey and R. S. Baty, Physics of Fluids **31**, 086106 (2019).
[56]J. F. Giron, S. D. Ramsey, and R. S. Baty, Physical Review E **101**, 053101 (2020).
[57]I. Giron, S. Balberg, and M. Krief, Physics of Fluids **33**, 066105 (2021).
[58]A. Velikovich and J. Giuliani, Physical Review E **98**, 013105 (2018).
[59]C. Huete, A. L. Velikovich, D. Martínez-Ruiz, and A. Calvo-Rivera, Journal of Fluid Mechanics **927** (2021).
[60]J. Grun, S. Obenschain, B. Ripin, R. Whitlock, E. McLean, J. Gardner, M. Herbst, and J. Stamper, The Physics of Fluids **26**, 588 (1983).
[61]M. Karasik, J. Weaver, Y. Aglitskiy, T. Watari, Y. Arikawa, T. Sakaiya, J. Oh, A. Velikovich, S. Zalesak, J. Bates, *et al.*, Physics of Plasmas **17**, 056317 (2010).
[62]J. D. Lindl, *Inertial confinement fusion: the quest for ignition and energy gain using indirect drive* (American Institute of Physics, 1998).
[63]R. Craxton, K. Anderson, T. Boehly, V. Goncharov, D. Harding, J. Knauer, R. McCrory, P. McKenty, D. Meyerhofer, J. Myatt, *et al.*, Physics of Plasmas **22**, 110501 (2015).
[64]D. Ryutov, M. S. Derzon, and M. K. Matzen, Reviews of Modern Physics **72**, 167 (2000).
[65]J. L. Giuliani and R. J. Commisso, IEEE Transactions on Plasma Science **43**, 2385 (2015).
[66]A. Beresnyak, A. L. Velikovich, J. L. Giuliani, and A. Dasgupta, Journal of Fluid Mechanics **936** (2022).
[67]C. A. Coverdale, C. Deeney, A. Velikovich, J. Davis, R. Clark, Y. Chong, J. Chittenden, S. Chantrenne, C. Ruiz, G. Cooper, *et al.*, Physics of Plasmas **14**, 056309 (2007).
[68]Y. Maron, A. Starobinets, V. Fisher, E. Kroupp, D. Osin, A. Fisher, C. Deeney, C. Coverdale, P. Lepell, E. Yu, *et al.*, Physical Review Letters **111**, 035001 (2013).
[69]A. Velikovich, M. Murakami, B. Taylor, J. Giuliani, S. Zalesak, and Y. Iwamoto, Physics of Plasmas **23**, 052706 (2016).
[70]W. Fickett and W. C. Davis, *Detonation: theory and experiment* (Courier Corporation, 2000).
[71]J. H. Lee, *The detonation phenomenon* (Cambridge University Press, 2008).
[72]J. Shepherd, Proceedings of the Combustion Institute **32**, 83 (2009).
[73]P. Clavin and F. A. Williams, Philosophical Transactions of the Royal Society A: Mathematical, Physical and Engineering Sciences **370**, 597 (2012).
[74]E. Vishniac, The Astrophysical Journal **274**, 152 (1983).
[75]V. Ktitorov, Voprosi Atomnoi Nauki I Tekhniki, Ser. Teoretich-eskaya i Prikladnaya Fizika (Atomic Science and Technology Issues, Ser. Theoretical and Applied Physics, in Russian) No. 2 , 28 (1984).
[76]J. Grun, J. Stamper, C. Manka, J. Resnick, R. Burris, J. Crawford, and B. H. Ripin, Phys. Rev. Lett. **66**, 2738 (1991).
[77]J. Sanz, S. Bouquet, C. Michaut, and J. Miniere, Physics of Plasmas **23**, 062114 (2016).
[78]R. P. Drake and F. W. Doss, The Astrophysical Journal **868**, 23 (2018).
[79]J. Minière, S. Bouquet, C. Michaut, J. Sanz, and M. Mancini, Astronomy & Astrophysics **617**, A133 (2018).
[80]D. Ryu and E. T. Vishniac, The Astrophysical Journal **313**, 820 (1987).
[81]J. H. Gardner, D. L. Book, and I. B. Bernstein, Journal of Fluid Mechanics **114**, 41 (1982).
[82]M. Murakami, J. Sanz, and Y. Iwamoto, Physics of Plasmas **22**, 072703 (2015).
[83]A. Roberts, *See National Technical Information Service Document PB2004-100597 [A. E. Roberts, Los Alamos Scientific Laboratory Report No. LA-299 1945 (unpublished)]* (Copies may be ordered from National Technical Information Service, Springfield, VA 22161, 1945).
[84]J. W. Bates, Physical Review E **69**, 056313 (2004).
[85]L. Landau and E. Lifshitz, *Fluid Mechanics. Second Edition* (Pergamon Press, Oxford, New York, 1987).
[86]P. Clavin and G. Searby, *Combustion waves and fronts in flows: flames, shocks, detonations, ablation fronts and explosion of stars* (Cambridge University Press, 2016).
[87]J. J. Erpenbeck, Phys. Fluids **5**, 1181 (1962).
[88]N. M. Kuznetsov, Dokl. Akad. Nauk SSSR **277**, 65 (1984), English translation Sov. Phys. Dokl. **29**, 532.
[89]N. M. Kuznetsov, Soviet Physics Uspekhi **32**, 993 (1989).
[90]R. Menikoff and B. J. Plohr, Review of Modern Physics **61**, 75 (1989).
[91]N. Freeman, Proceedings of the Royal Society of London. Series A. Mathematical and Physical Sciences **228**, 341 (1955).
[92]P. Zaidel', Journal of Applied Mathematics and Mechanics **24**, 316 (1960).
[93]G. Fowles and G. Swan, Physical Review Letters **30**, 1023 (1973).
[94]J. Wouchuk and J. L. Cavada, Physical Review E **70**, 046303 (2004).
[95]J. Bates, Physical Review E **91**, 013014 (2015).
[96]R. Marshak, The Physics of Fluids **1**, 24 (1958).
[97]K. Shimamura, J. A. Ofosu, M. Fukunari, and K. Komurasaki, in *2013 19th IEEE Pulsed Power Conference (PPC)* (IEEE, 2013) pp. 1–5.

[98]J. Urzay, Annual Review of Fluid Mechanics **50**, 593 (2018).
[99]C. Huete, A. Cuadra, M. Vera, and J. Urzay, Physics of Fluids **33**, 086111 (2021).
[100]M. Slemrod, Archive for Rational Mechanics and Analysis **81**, 301 (1983).
[101]M. S. Cramer and R. Sen, The Physics of fluids **30**, 377 (1987).
[102]L. He and P. Clavin, Journal of fluid mechanics **277**, 227 (1994).
[103]P. Clavin and B. Denet, Journal of Fluid Mechanics **897** (2020).
[104]Y. B. Zeldovich, Zh. Eksp. Teor. Fiz **12**, 389 (1942).
[105]G. I. Taylor, Proceedings of the Royal Society of London. Series A. Mathematical and Physical Sciences **200**, 235 (1950).
[106]A. Liñán, V. N. Kurdyumov, and A. L. Sánchez, Comptes Rendus Mécanique **340**, 829 (2012).